2

Molybdenum / Chromium Complexes for Carbon Dioxide, Sodium Bicarbonate and Inorganic Carbonate Hydrogenation to Formates

2(a) Molybdenum Catalyzed Hydrogenation of Carbon Dioxide, Bicarbonate, and Inorganic Carbonates to Formates

Research Article based on this study:

Singh, T.; Chakraborty, S. Molybdenum-Catalyzed Hydrogenation of Carbon Dioxide, Bicarbonate, and Inorganic Carbonates to Formates. *Dalton Trans.* **2024**, *53*, 10244-10249.

2(a).1 Introduction

Homogeneous catalytic hydrogenation mediated by transition metal complexes is an atom-economic and sustainable process practiced in industry and academia.[177] Recent years have witnessed remarkable progress in this direction spearheaded by Noyori, Shvo, Milstein, Beller, and others.[136,178,179,181] Nevertheless, the complexes explored in these reactions are derived from precious late-transition metals suffering from scarcity and toxicity issues. Contemporary investigation spotlights 3d transition metal complexes in homogeneous catalysis in view of their natural abundance, low-toxicity, and cost-effectiveness.[11,12,50,53,55,56] In this regard non-noble, non-precious molybdenum-based complexes are also attractive replacements of platinum group metals owing to their bio-compatibility and earth-abundance.[182,183] In fact, Mo catalysis has been exploited in a large number of synthetically relevant reactions including oxidation, metathesis reactions, and reduction of nitrogen to ammonia.[182,184-186]However, complexes of Mo have sparsely been investigated in homogeneous hydrogenation reactions.[183,187-190] Lately, there has been a resurgence of Mo hydrogenation catalysis with the appearance of reports on olefin hydrogenation, semi-hydrogenation of alkynes, aldehydes, ketones, imines, nitriles, and amides hydrogenation including heteroaromatics.[192-201] We have reviewed group VI metals catalyzed (de)hydrogenation reactions.[202] Very recently Jiao, Junge, and Beller described Mo carbene complexes catalyzed hydrogenation of esters.[203]

In this context, the hydrogenation of carbon dioxide is also an appealing transformation. CO_2 is one of the most notorious greenhouse gases evolved while the depletion of fossil fuels causing global warming.[15] Carbon dioxide being an inexpensive, innocuous, and earth-abundant C1 source, has the potential to serve as sustainable feedstock and cost-effective raw materials for the manufacture of bulk and fine chemicals.[23]Hydrogenating CO_2 to formic acid is highly desirable in light of the multi-fold utility of formic acid and for the production of plasticizers, varnishes, resins, and glass etc.[29] In addition, CO_2 hydrogenation to formic acid/formate is promising considering its application as a potential liquid hydrogen carrier within the framework of 'Circular economy'.[24,67] Nonetheless, activation of CO_2 is difficult because of thermodynamic stability and kinetic inertness. The CO_2 and H_2 reaction is endergonic ($G°_{298}$ = +32.8 kJ mol^{-1}) requiring a base to make the overall process thermodynamically downhill. Regardless of the challenges associated with CO_2 hydrogenation, significant breakthroughs have been made in the realm of transition metal-catalyzed CO_2 hydrogenation to formic acid/formate including earth-abundant 3d base

metals.[39,44,45,49,87,88,92,95,100,101,102,106,107,111,112,113,116,121,122,124,126,202,204,205] However, very less attention have been paid on CO_2 hydrogenation by Mo complexes. Berke group in 2015 attempted the PNP pincer Mo catalyzed CO_2 hydrogenation achieving formate with a very low yield of 4% (Figure 3.1).[129] Bernskoetter utilized the triphos complex (κ^4 -$PN^{Me}P$)-Mo(C_2H_4)(κ^2-O_2CH) and hydrogenated CO_2 to formate with a TON of 35.[130] Lately, Hawkins and co-workers reported heterobimetallic Mo/Ir catalyzed hydrogenation of CO_2 to formate and a TON of 128 was reported.[132] In 2020, computational studies by Liu and Ke[131] on group VI NHC-supported complexes revealed that low electronegativity and low oxidation state complexes can be effective catalysts for CO_2 hydrogenation. Prompted by this study, we delve into the CO_2 hydrogenation using Mo catalysts bearing bidentate phosphine ligands with varied bite angles. We report here Mo catalyzed CO_2, sodium bicarbonate, and inorganic carbonate hydrogenation to formate utilizing bis-phosphine Mo complexes. To the best of our knowledge, there are no reports on carbonate and bicarbonate hydrogenation using Mo complexes thus far.

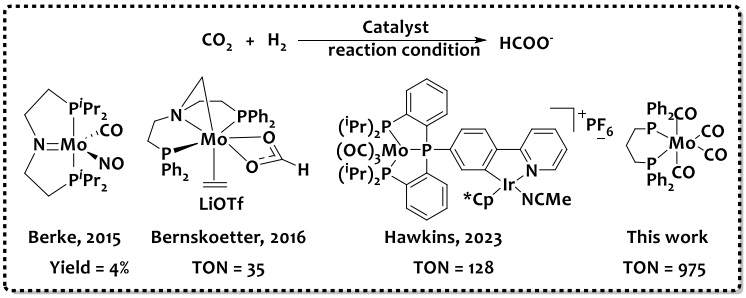


Fig. 2(a).1 Molybdenum catalysts known for CO_2 hydrogenation.

2(a).2 Results & Discussion

Our initial focus was to assess the catalytic activity of several small, natural, and large bite angle (β_n = 72-111°)[30] bidentate phosphine-based Mo complexes for the task. Employing wide bite angle phosphine complexes in catalysis is intriguing as these ligands impart unique reactivity via their electronics and steric bulk.[206-208]

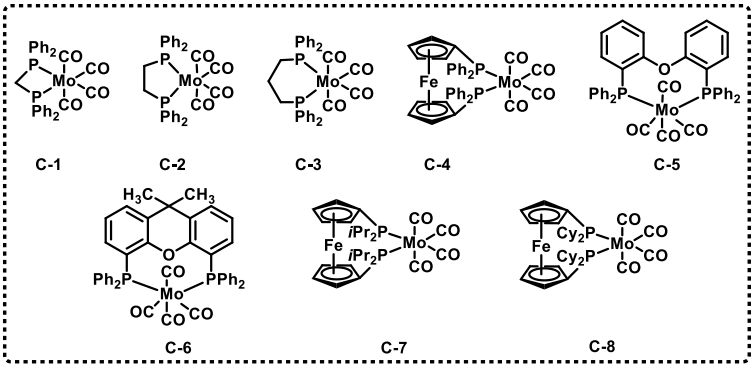
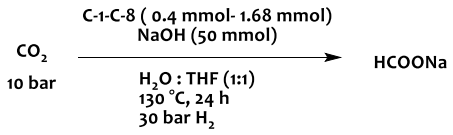


Fig. 2(a).2 Molybdenum complexes tested for CO_2 hydrogenation.

Hence complexes **C-1- C-8** (Figure 2(a).2) were prepared according to literature procedures.[209-211] At the outset 1.68 μmol small bite angle DPPM (1,1-Bis(diphenylphosphino)methane, β_n=72°) ligand-based complex **C-1** was used for CO_2 hydrogenation in combination with 50 mmol NaOH at 130°C in THF/H_2O with 40 bar (CO_2:H_2 = 1:3) pressure producing formate with a TON of 53 (Table 2(a).1, entry 1). When 1.64 μmol Mo(DPPE)$(CO)_4$ (DPPE=1,2-Bis(diphenylphosphino)ethane, β_n = 85°) (**C-2**) was taken as catalyst, formate was obtained with a TON of 85 (Table 2(a).1, entry 2). To our delight, natural bite angle DPPP (1,3-Bis(diphenylphosphino)propane) (91°) supported complex Mo(DPPP)$(CO)_4$ (0.40 μmol, **C-3**) catalyzed CO_2 hydrogenation affording formate with a

maximum TON of 975 (Table 2(a).1, entry 3). However, $Mo(DPPF)(CO)_4$ (**C-4**, DPPF = 1,1′-Bis(diphenylphosphino)ferrocene (96°), 1.31 μmol) furnished formate with a low TON of 22 (Table 2(a).1, entry 4). Shifting the catalytic system towards large bite angle DPEphos (103°) and Xantphos (111°)-based complexes **C-5** (1.34 μmol) and **C-6**, (1.27 μmol) did not show any improvement on CO_2 hydrogenation yielding formates with TONs of 156 and 275, respectively (Table 2(a).1, entries 5,6). A blank reaction was also carried out without catalysts. As expected, trace amount of formate formation was observed in this case (Table 2(a).1, entry 7).

Table2(a).1 Molybdenum catalyzed CO_2 hydrogenation to formate.[a]



Entry	Base	Cat (μmol)	Time	Solvent	TON[b]
1	NaOH	C-1(1.68)	24h	THF:H_2O	53
2	NaOH	C-2(1.64)	24h	THF:H_2O	85
3	NaOH	C-3(0.40)	24h	THF:H_2O	975
4	NaOH	C-4(1.31)	24h	THF:H_2O	22
5	NaOH	C-5(1.34)	24h	THF:H_2O	156
6	NaOH	C-6(1.27)	24h	THF:H_2O	275
7	NaOH	-	24h	THF:H_2O	Trace
8	NaOH	C-7(1.46)	24h	THF:H_2O	37
9	NaOH	C-8(1.27)	24h	THF:H_2O	511
10[c]	DBU	C-3(0.40)	24h	THF:H_2O	Trace
11[c]	Et_3N	C-3(0.40)	24h	THF:H_2O	Trace
12[c]	K_3PO_4	C-3(0.40)	24h	THF:H_2O	100
13	KOH	C-3(0.40)	24h	THF:H_2O	200
14	LiOH	C-3(0.40)	24h	THF:H_2O	625
15	$Ca(OH)_2$	C-3(0.40)	24h	THF:H_2O	362
16	NaOH	C-3(0.40)	12h	THF:H_2O	275
17	NaOH	C-3(0.40)	48h	THF:H_2O	975
18[d]	NaOH	C-3(0.40)	24h	THF:H_2O	475
19[e]	NaOH	C-3(0.40)	24h	THF:H_2O	275
20	NaOH	C-3(0.40)	24h	H_2O	Trace
21	NaOH	C-3(0.40)	24h	THF	225
22[f]	NaOH	C-3(0.40)	24h	THF:H_2O	575
23[g]	NaOH	C-3(0.40)	24h	THF:H_2O	350

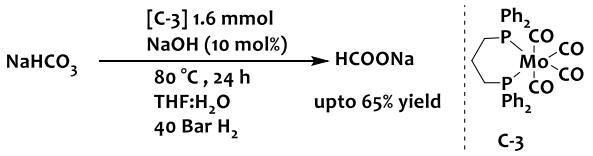
[a]Reaction conditions: Unless and otherwise stated 130 °C, 30 bar H_2 at room temperature, 10 bar CO_2, 24 h, 50 mmol NaOH, certain μmol catalyst. [b]Yield based on ^{1}H NMR signals of sodium formate, with DMF used as an internal standard. Turnover number = moles of sodium formate per mole of catalyst. [c]50 mmol respective bases and 0.1 mmol NaOH was used as additive. [d]0.1 mmol TMNO was taken. [e]Complex was exposed to UV light and then used as catalyst. [f]10:10 CO_2:H_2 was used. g5:15 CO_2:H_2 was used.

Next, we were curious to probe the effect of electronics on catalytic hydrogenation reaction. Accordingly, $Mo(DiPPF)(CO)_4$ **C-7** (1.46 μmol; DiPPF = 1,1′-Bis(diisopropylphosphino)ferrocene; β_n = 103.6) and $Mo(DCPF)(CO)_4$ (1.27 μmol; DCPF = 1,1′-Bis(dicyclohexylphosphino)ferrocene; β_n =102.4) **C-8** were employed as catalysts and TONs of 37 and 511 were observed, respectively (Table 2(a).1, entries 8-9). These studies indicate the crucial role of varied bite angle and phosphine substituents may have in tuning the catalytic

performance of the complex. With the most active catalyst **C-3** in hand, base screening was done under optimum conditions. Surprisingly, when DBU and Et_3N were utilized as bases, trace amount of respective formate salts was formed (Table 2(a).1, entries 10-11). However, usage of K_3PO_4 as base in the reaction mixture resulted in formation of the corresponding formate with a TON of 100 (Table 2(a).1, entry 12). Use of KOH and LiOH as bases resulted in the formate formation with TONs of 200 and 625, respectively (Table 2(a).1, entries 13-14). Ca(OH)2 was also tested as base in the reaction and a TON of 362 was achieved (Table 2(a).1, entry 15). On reducing the reaction time to 12 h the TON significantly dropped to 275 (Table 2(a).1, entry 16) whereas no further increase in TON was noticed when the reaction was carried out for 48 h (Table 2(a).1, entry 17) presumably due to catalyst decomposition. We also attempted to generate the active catalytically active species by thermal (trimethylamine N-oxide; TMNO) and photolytic elimination of CO (Table 2(a).1, entries 18 and 19). However, no marked improvement on yields of formate formation was observed. Solvent optimization was also performed by carrying out the reaction in neat THF and water independently. Trace amount of formate was obtained using water as a solvent. Interestingly, TON of 225 was recorded when only THF was used (Table 2(a).1, entries 20-21), inferring the role of THF solvent in stabilizing the catalytically active intermediates. Decreasing the total gaseous pressure to 20 bar under optimum condition, a lower TON for the corresponding formate formation was observed (Table 2(a).1, entries 22 and 23).

Next, we examined the catalytic performance of **C-3** in the hydrogenation of sodium bicarbonate and inorganic carbonates.[212-213] Excitingly, 1.6 µmol **C-3** in concoction with 10 mol% NaOH, at 80 °C after 24h in THF/H_2O in the presence of 40 bar H_2 hydrogenated sodium bicarbonate to sodium formate with a yield of 64% (Table 2(a).2, entry 1). Reducing the H_2 pressure to 20 bar afforded lower formate yield of 27.5% (Table 2(a).2, entry 2). Applying 10 mol% *t*-BuOK in place of NaOH for generating active catalyst resulted in formate formation with 54% yield (Table 2(a).2, entry 3). Increasing the temperature to 130 °C resulted in 29% formate yield (Table 2(a).2, entry 4). Trace amount of formate was obtained without any catalyst loading (Table 2(a).2, entry 5). Carrying out the reaction without an external base furnished formate with 18.5% yield (Table 2(a).2, entry 6).

Table2(a).2 Molybdenum catalyzed hydrogenation of sodium bicarbonate.[a]

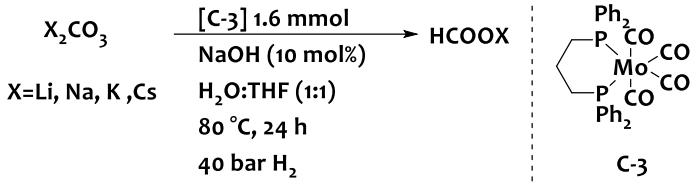


Entry	Base	Catalyst	Pressure	Solvent
1	NaOH	**C-3**	40 bar	THF:H_2O
2	^{t}BuOK	**C-3**	20 bar	THF:H_2O
3	NaOH	**C-3**	40 bar	THF:H_2O
4[c]	NaOH	**C-3**	40 bar	THF:H_2O
5	-	**-**	40 bar	THF:H_2O
6	-	**C-3**	40 bar	THF:H_2O

[a]Reaction conditions: $NaHCO_3$ 0.5 mmol, 80 °C, 40 bar H_2, 24 h, 1.6 µmol catalyst (**C-3**), 10 mol% NaOH. [b]Yield based on ^{1}H NMR signals of sodium formate with DMF used as an internal standard. [c]Reaction was heated to 130 °C.

C-3 was also applied for inorganic carbonate hydrogenation. Lithium carbonate was hydrogenated to its corresponding formate with a yield of 65% using 1.6 µmol **C-3** in conjunction with 10 mol% NaOH at 80° C in THF/H_2O after 24 h under 40 bar H_2 (Table 2(a).3, entry 1). **C-3** also exhibited catalytic activity towards sodium carbonate, potassium carbonate, and caesium carbonate to the corresponding formats albeit very low yields (Table 2(a).3, entries 2-4). The dependence of the catalytic performance on the nature of the cation might be related to the physicochemical properties of the salt.[100] Recently, Beller group reported Mn catalyzed carbonate hydrogenation by varying the cations and the best formate yield was obtained in case of Li_2CO_3.[213] A hydrogenation reaction of lithium carbonate was also conducted catalyzed by **C-3** in the absence of NaOH additive yielding lower amount of the corresponding formate product (19% , Table 2(a).3, entry 5) indicating the crucial role of NaOH in generating the catalytically active species.

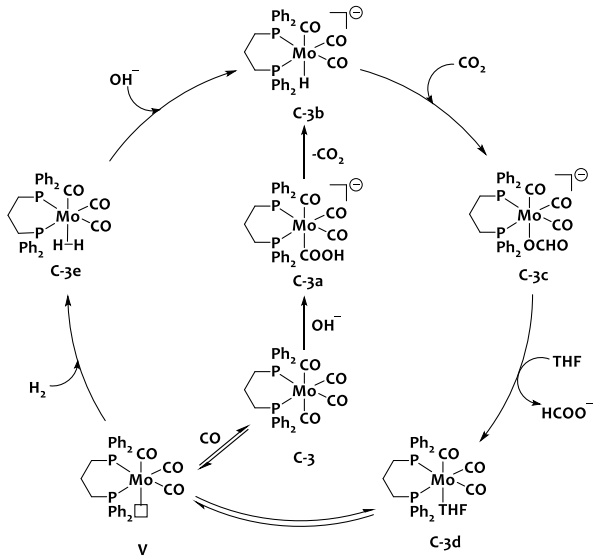
Table2(a).3 Molybdenum catalyzed inorganic carbonate hydrogenation.[a]



Entry	Base	Catalyst	Solvent	Yield[b]	X
1	NaOH	**C-3**	THF:H_2O	65%	Li
2	NaOH	**C-3**	THF:H_2O	0.5%	Na
3	NaOH	**C-3**	THF:H_2O	2.5%	K
4	NaOH	**C-3**	THF:H_2O	2%	Cs
5[c]	NaOH	**C-3**	THF:H_2O	19%	Li

[a]Reaction conditions: X2CO3 (X= Li, Na, K, Cs) 0.5 mmol, 80 oC, 40 bar H_2 at room temperature, 24 h, 1.6 µmol catalyst (C-3), 10 mol% NaOH. [b]Yields based on ^{1}H NMR signals of sodium formate with DMF used as an internal standard.[c] No NaOH was used.

Aiming to gain insights into Mo-catalyzed CO_2 hydrogenation reactions, preliminary experiments were carried out. Initially, when 5 eq. NaOH was added to a THF solution of **C-3** and heated to 130 °C for 3 h, transparent solution turned into light orange colour. A new peak at 10 ppm was observed in the ^{1}H NMR spectrum.[214-216] This could be due to the formation of metallacarboxylate complex **C-3a** (Scheme 2(a).1). Downfield ^{1}H NMR shift of the hydroxycarbonyl ligand for related Ir and Pt complexes have been observed.[215-216] Notably, a new signal at 29.4 ppm in ^{31}P NMR appeared along with the free ligand peak at -22 ppm indicating the formation of **C-3a** along with the decomposition of catalyst in the presence of excess NaOH. Additionally, IR spectroscopy supports the formation of a carboxylate intermediate **C-3a** (Scheme 2(a).1). Further, heating the reaction mixture overnight, a new signal at 8.5 ppm in the ^{1}H NMR spectroscopy appeared, which is identified as formate signal. Formation of a formate complex **C-3c** (Scheme 2(a).1)was further corroborated by HRMS. Surprisingly, negligible change in ^{31}P NMR was observed in this case. A mercury poisoning test was also carried out by introducing a drop of mercury in the reaction mixture and benchmark reaction did not experience significant dip in TON (900), which confirms the homogeneous nature of reaction.



Scheme 2(a).1 Proposed mechanism for **C-3** catalyzed CO_2 hydrogenation.

Based on the observation, we propose a mechanism as depicted in (Scheme 2(a).1). The reaction proceeds via the formation of a metallacarboxylate **C-3a** formed by the nucleophilic attack of NaOH on **C-3**.[127-128] **C-3a** is converted into a formato complex **C-3c** via complex transient hydride species **C-3b**. **C-3c** in the presence of base yielded formate and **C-3d**, which coordinates with dihydrogen giving rise to **C-3f**. Deprotonation of **C-3f** with NaOH regenerates hydride **C-3b** completing the catalytic cycle. An alternative pathway as described in Scheme 1 might also be plausible in which the H_2 added complex **C-3f** is formed by the elimination of CO from **C-3** forming a 16-e complex **C-3e**.[217-218]

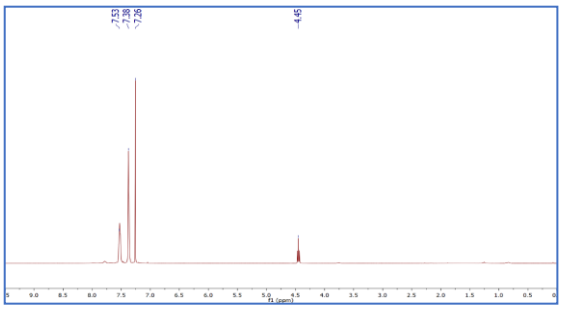
2(a).3 Experimental Section

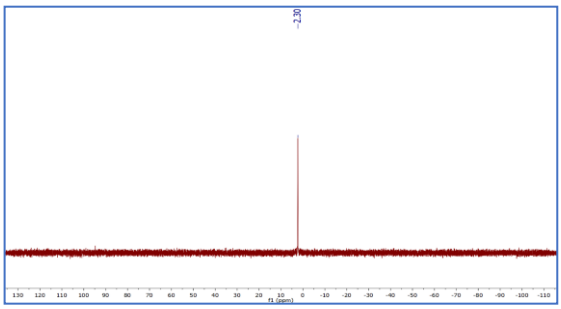
The complexes **C-1** to **C-8** were synthesized by charging the Schlenk flask with $Mo(CO)_6$ and toluene solution of respective phosphine ligands in equimolar ratio inside the glove box. The reaction mixture was heated at 120 °C for 48 hours. Afterwards, reaction was stopped, cooled and solvent was dried under vacuum. Fine powder thus obtained were characterized. Data obtained was found in accordance with the reported literatures.[209-211]

2(a).3.1 Representative Characterization Data for Complex C-1

$MoDPPM(CO)_4$ (**C-1**)
^{1}H NMR (500 MHz, $CDCl_3$) δ 7.53-7.26m(Ar), 4.45(t).
^{31}P{^{1}H}-NMR (203.0 MHz, $CDCl_3$) δ 2.3 (s, 2P).
FT-IR cm^{-1} ν(CO) 2016, 1912, 1857.
HRMS $C_{29}H_{22}MoO_4P_2$ Calculated 594.0047. Found 594.1570.

(a)

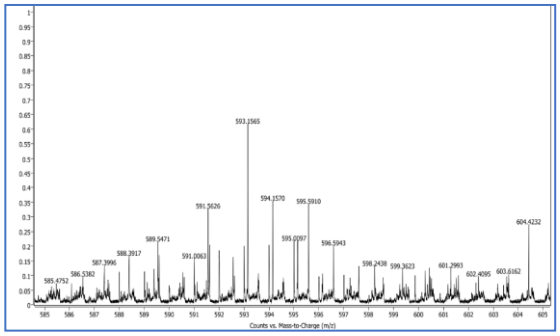


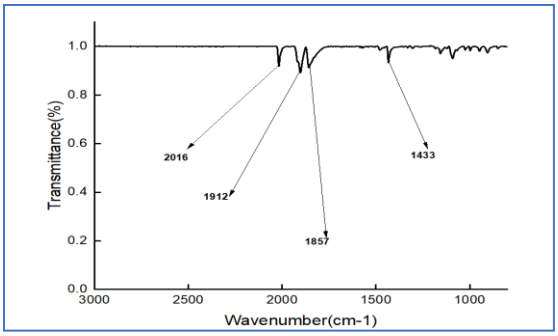


(b)

Fig. 2(a).3.1 (a) ^{1}H NMR Spectrum, **(b)** ^{31}P Spectrum for **C-1** complex.

(c)





(d)

Fig. 2(a).3.1 (c) ESI-MS Spectrum, **(d)** FTIR Spectrum for **C-1** complex.

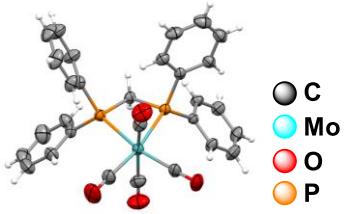


Fig. 2(a).3.1 (e) ORTEP Drawing of **C-1** complex.

Table 2(a).4 Crystal data and structure refinement for **C-1.**

Ccdc no.	2241306
Empirical formula	$C_{29}H_{22}MoO_4P_2$
Formula weight	592.34
Temperature/K	298
Crystal system	monoclinic
Space group	$P2_1/c$
a/Å	16.405(3)
b/Å	9.5092(14)
c/Å	18.135(3)
α/°	90
β/°	103.336(6)
γ/°	90
Volume/Å^3	2752.8(8)
Z	4
ρ_{calc}g/cm^3	1.429
μ/mm^{-1}	0.624
F(000)	1200.0
Crystal size/mm^3	0.231 × 0.098 × 0.078
Radiation	MoKα (λ = 0.71073)
2Θ range for data collection/°	4.616 to 49.996
Index ranges	-19 ≤ h ≤ 19, -11 ≤ k ≤ 11, -21 ≤ l ≤ 21
Reflections collected	50748
Independent reflections	4836 [R_{int} = 0.1448, R_{sigma} = 0.0658]
Data/restraints/parameters	4836/0/325
Goodness-of-fit on F^2	1.028
Final R indexes [I>=2σ (I)]	R_1 = 0.0397, wR_2 = 0.0714
Final R indexes [all data]	R_1 = 0.0932, wR_2 = 0.0923

2(a).3.2 Representative Characterization Data for Complex C-2

$MoDPPE(CO)_4$ (**C-2**)
^{1}H NMR (500 MHz, $CDCl_3$) δ 7.64-7.31 m(Ar), 2.48 m(2H), 2.45 m(2H).
$^{31}P\{^1H\}$-NMR (203.0 MHz, $CDCl_3$) δ 55.2 (2P).
FT-IR cm^{-1} ν(CO) 2013, 1902, 1869.
HRMS $C_{30}H_{24}MoO_4P_2$ Calculated 608.0204. Found 608.6085.

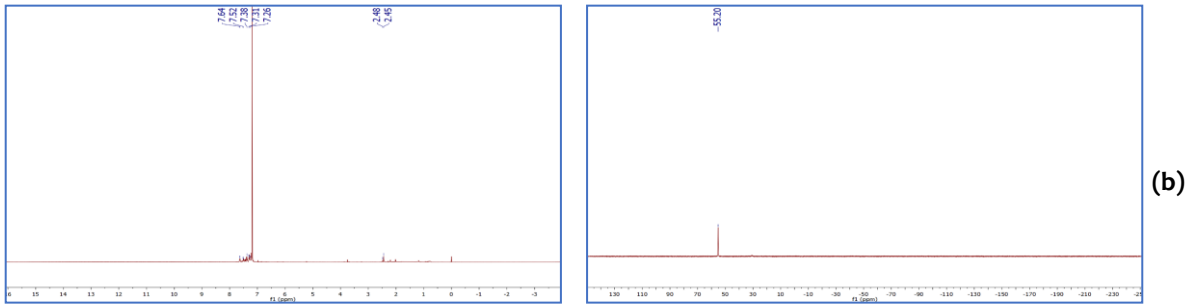


Fig. 2(a).3.2 (a) ^{1}H NMR Spectrum, **(b)** ^{31}P Spectrum for **C-2** complex.

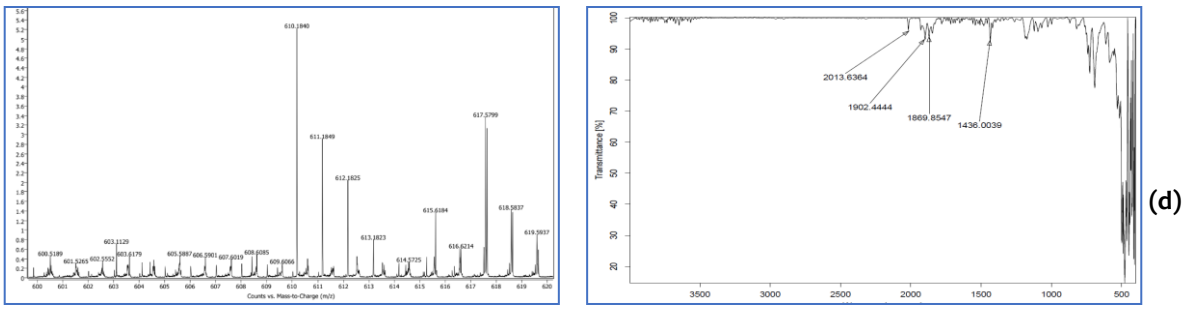


Fig. 2(a).3.2 (c) ESI-MS Spectrum, **(d)** FTIR Spectrum for **C-2** complex.

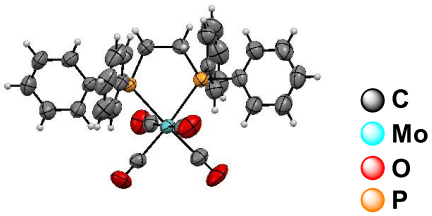


Fig. 2(a).3.2 (e) ORTEP Drawing of **C-2** complex.

Table 2(a).5 Crystal data and structure refinement for **C-2.**

Ccdc no.	2241303
Empirical formula	$C_{30}H_{24}MoO_4P_2$
Formula weight	606.37
Temperature/K	298
Crystal system	orthorhombic
Space group	Pbca
a/Å	16.8125(14)
b/Å	14.6185(12)
c/Å	22.679(2)
α/°	90

β/°	90
γ/°	90
Volume/Å^3	5573.9(8)
Z	8
ρ_{calc}g/cm^3	1.445
μ/mm^{-1}	0.619
F(000)	2464.0
Crystal size/mm^3	0.145 × 0.125 × 0.086
Radiation	MoKα (λ = 0.71073)
2Θ range for data collection/°	5.152 to 52.824
Index ranges	-21 ≤ h ≤ 21, -17 ≤ k ≤ 18, -28 ≤ l ≤ 28
Reflections collected	96953
Independent reflections	5714 [R_{int} = 0.1140, R_{sigma} = 0.0401]
Data/restraints/parameters	5714/0/335
Goodness-of-fit on F^2	1.066
Final R indexes [I>=2σ (I)]	R_1 = 0.0366, wR_2 = 0.0835
Final R indexes [all data]	R_1 = 0.0698, wR_2 = 0.1042
Largest diff. peak/hole / e Å^{-3}	0.53/-0.56

2(a).3.3 Representative Characterization Data for Complex C-3

MoDPPP(CO)$_4$ (**C-3**)
^{1}H NMR (500 MHz, $CDCl_3$) δ 7.39-7.19 m(Ar), 2.38m(4H), 1.90(2H).
^{31}P{^{1}H}-NMR (203.0 MHz, $CDCl_3$) δ 21.23 (2P).
FT-IR cm^{-1} ν(CO) 2016, 1905, 1856.
HRMS $C_{31}H_{26}MoO_4P_2$ Calculated 622.0360. Found 622.0264.

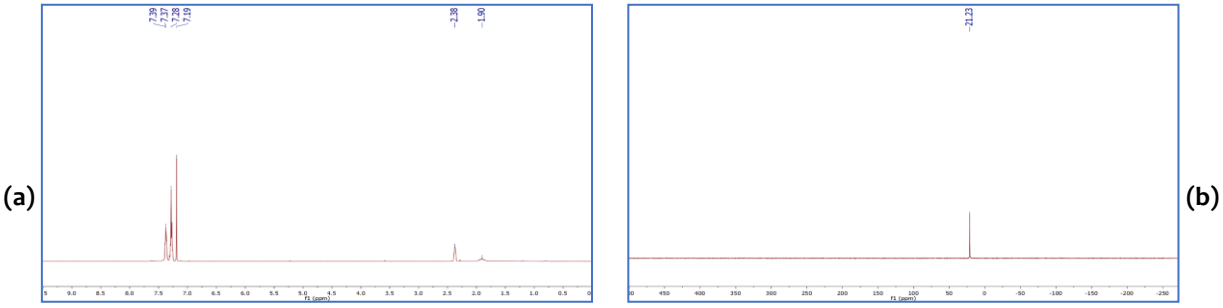


Fig.2(a).3.3 (a) ^{1}H NMR Spectrum, **(b)** ^{31}P Spectrum for **C-3**

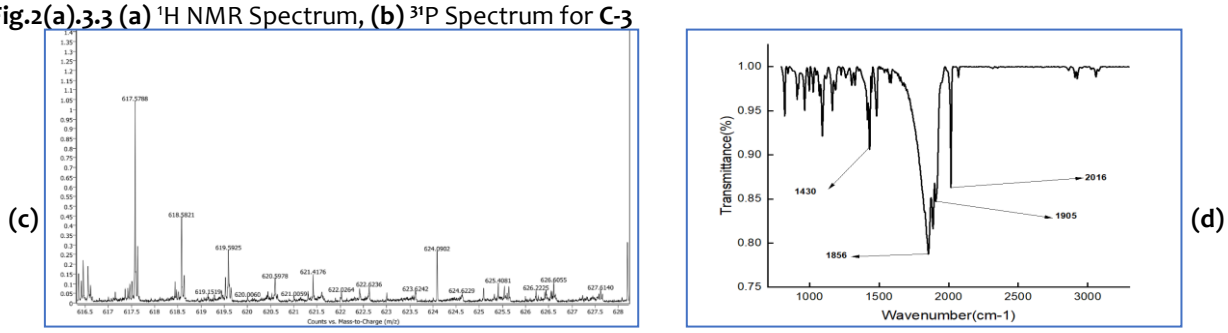


Fig. 2(a).3.3 (c) ESI-MS Spectrum, **(d)** FTIR Spectrum for **C-3** complex.

2(a).3.4 Representative Characterization Data for Complex C-4

$MoDPPF(CO)_4$ (**C-4**)
^{1}H NMR (500 MHz, $CDCl_3$) δ 7.26-7.60 m(Ar), 4.25m (8H).
$^{31}P\{^1H\}$-NMR (203.0 MHz, $CDCl_3$) δ 33.24 (2P).
FT-IR cm^{-1} ν(CO) 2020, 1891, 1878.
HRMS $C_{40}H_{34}FeMoO_4P_2$ Calculated 794.0330. Found 794.8298.

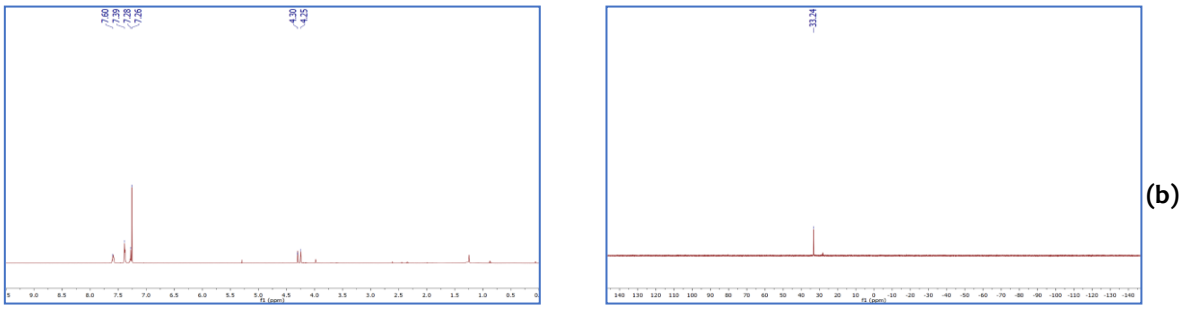


Fig. 2(a).3.4 (a) ^{1}H NMR Spectrum, **(b)** ^{31}P Spectrum for **C-4** complex.

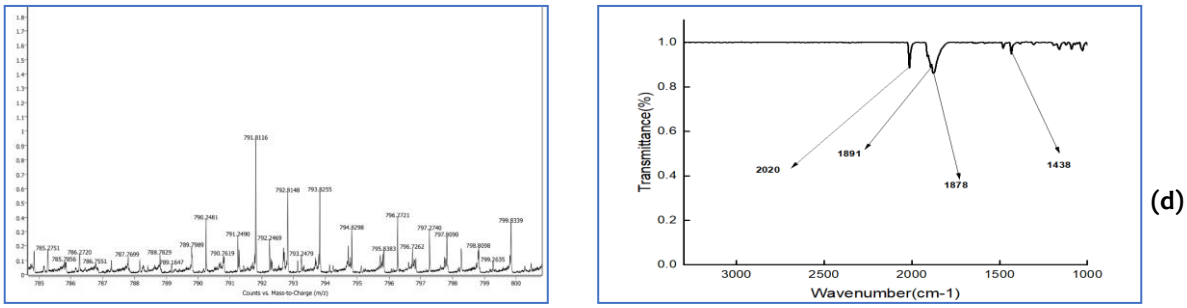


Fig. 2(a).3.4 (c) ESI-MS Spectrum, **(d)** FTIR Spectrum for **C-4** complex.

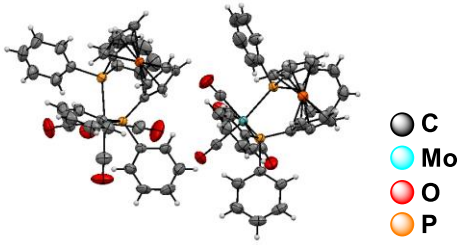


Fig. 2(a).3.4 (e) ORTEP Drawing of **C-4** complex.

Table2(a).6 Crystal data and structure refinement for **C-4**

Ccdc no.	2241308
Empirical formula	$C_{38}H_{28}FeMoO_4P_2$
Formula weight	762.33
Temperature/K	298.0
Crystal system	monoclinic
Space group	$P2_1/n$
a/Å	9.3770(7)
b/Å	34.898(3)
c/Å	20.4468(16)
α/°	90
β/°	92.627(3)

γ/°	90
Volume/Å^3	6684.0(9)
Z	8
ρ_{calc}g/cm^3	1.515
μ/mm^{-1}	0.945
F(000)	3088.0
Crystal size/mm^3	0.236 × 0.156 × 0.123
Radiation	MoKα (λ = 0.71073)
2Θ range for data collection/°	4.502 to 50.892
Index ranges	-11 ≤ h ≤ 11, -42 ≤ k ≤ 42, -24 ≤ l ≤ 24
Reflections collected	87639
Independent reflections	12259 [R_{int} = 0.0926, R_{sigma} = 0.0515]
Data/restraints/parameters	12259/0/829
Goodness-of-fit on F^2	1.035
Final R indexes [I>=2σ (I)]	R_1 = 0.0338, wR_2 = 0.0689
Final R indexes [all data]	R_1 = 0.0543, wR_2 = 0.0776
Largest diff. peak/hole / e Å^{-3}	0.34/-0.35

2(a).3.5 Representative Characterization Data for Complex C-5

MoDPEPHOS(CO)$_4$ (**C-5**)
^{1}H NMR (500 MHz, $CDCl_3$) δ 7.40-6.87 m (22H), 6.50 t(2H).
^{31}P{^{1}H}-NMR (203.0 MHz, $CDCl_3$) δ 26.97 (2P).
FT-IR cm^{-1} ν(CO) 2024, 1922, 1867.
HRMS $C_{40}H_{28}MoO_5P_2$ Calculated 748.0466. Found 748.5423.

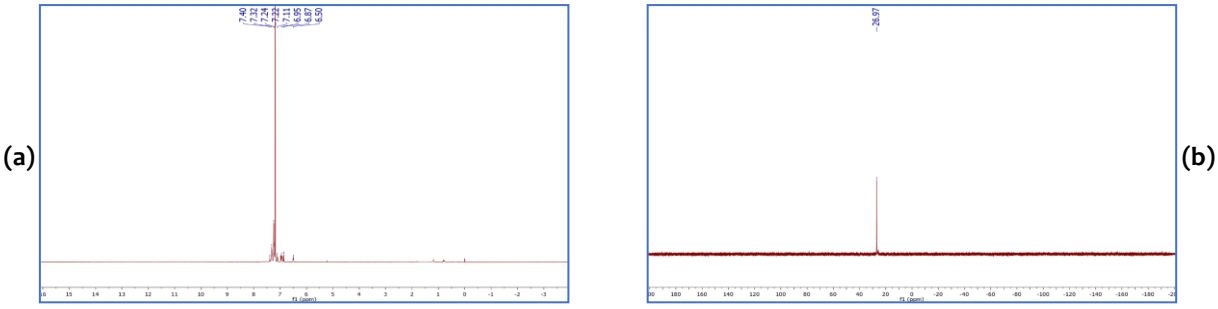


Fig. 2(a).3.5 (a) ^{1}H NMR Spectrum, **(b)** ^{31}P Spectrum for **C-5** complex.

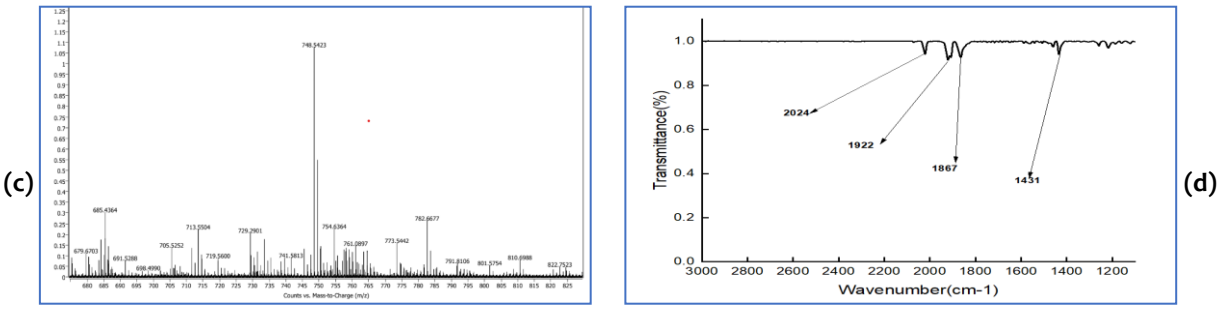


Fig. 2(a).3.5 (c) ESI-MS Spectrum, **(d)** FTIR Spectrum for **C-5** complex.

2(a).3.6 Representative Characterization Data for Complex C-6

MoXanthphos(CO)$_4$ (**C-6**)

^{1}H NMR (500 MHz, $CDCl_3$) δ 7.47-6.97 m (22H), 6.54 t (2H), 1.56 t (6H).
^{31}P{^{1}H}-NMR (203.0 MHz, $CDCl_3$) δ 20.71 (2P).
FT-IR cm^{-1} ν(CO) 2013, 1913, 1862.
HRMS $C_{43}H_{32}MoO_5P_2$ Calculated 788.0779. Found 788.0768.

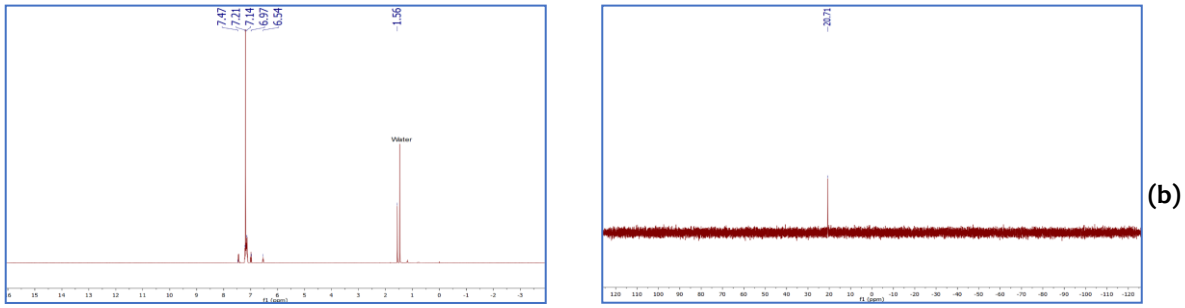


Fig. 2(a).3.6 (a) ^{1}H NMR Spectrum, **(b)** ^{31}P Spectrum for **C-6** complex.

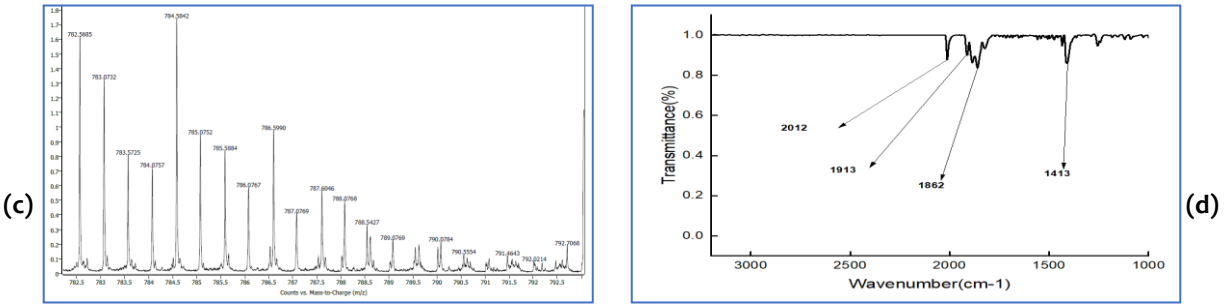


Fig. 2(a).3.6 (c) ESI-MS Spectrum, **(d)** FTIR Spectrum for **C-6** complex.

2(a).3.7 Representative Characterization Data for Complex C-7

$MoDiPPF(CO)_4$ (**C-7**)
^{1}H NMR (500 MHz, $CDCl_3$) δ 4.31 (4H), 4.16 (4H), 2.24 m (4H), 1.93-1.24 m (24H).
^{31}P{^{1}H}-NMR (203.0 MHz, $CDCl_3$) δ 41.25 (2P).
FT-IR cm^{-1} ν(CO) 2010, 1885, 1845.
HRMS $C_{26}H_{36}FeMoO_4P_2$ Calculated 628.0480. Found 628.0483.

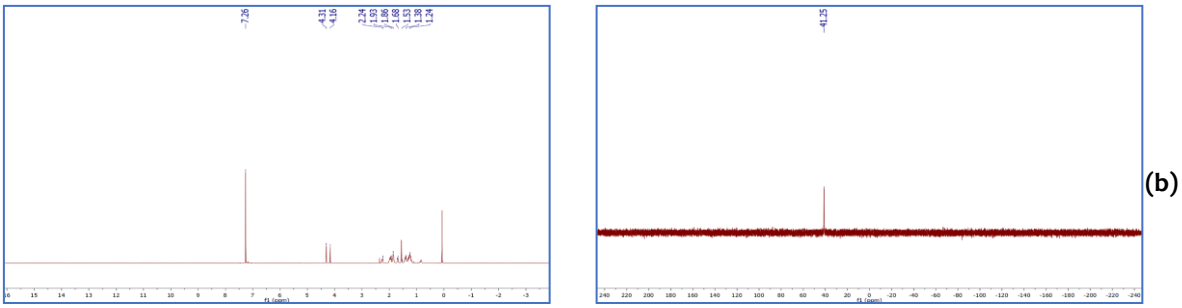


Fig. 2(a).3.7 (a) ^{1}H NMR Spectrum, **(b)** ^{31}P Spectrum for **C-7** complex.

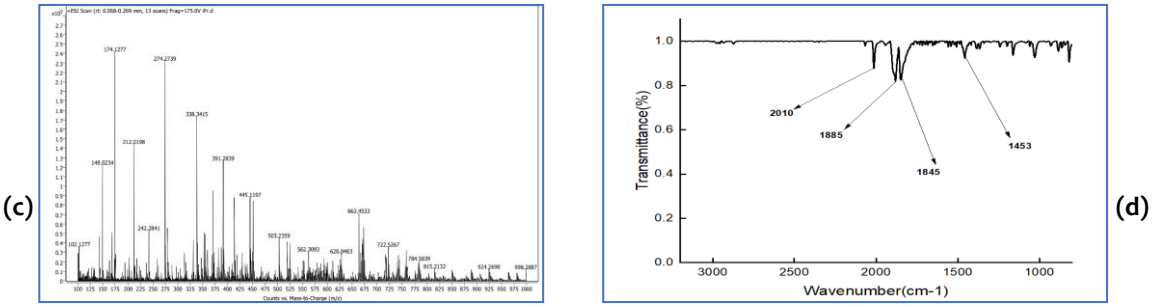


Fig. 2(a).3.7 (c) ESI-MS Spectrum, **(d)** FTIR Spectrum for **C-7** complex.

2(a).3.8 Representative Characterization Data for Complex C-8

$MoDCPF(CO)_4$ (**C-8**)
^{1}H NMR (500 MHz, $CDCl_3$) δ 4.34 (4H), 4.24 (4H), 2.31 (4H), 1.55 (4H), 1.30 m(20H), 1.20 m (16H).
^{31}P{^{1}H}-NMR (203.0 MHz, $CDCl_3$) δ 33.61 (2P).
FT-IR cm^{-1} ν(CO) 2012, 1857.
HRMS $C_{38}H_{52}FeMoO_4P_2$ Calculated 788.1738. Found 788.1741.

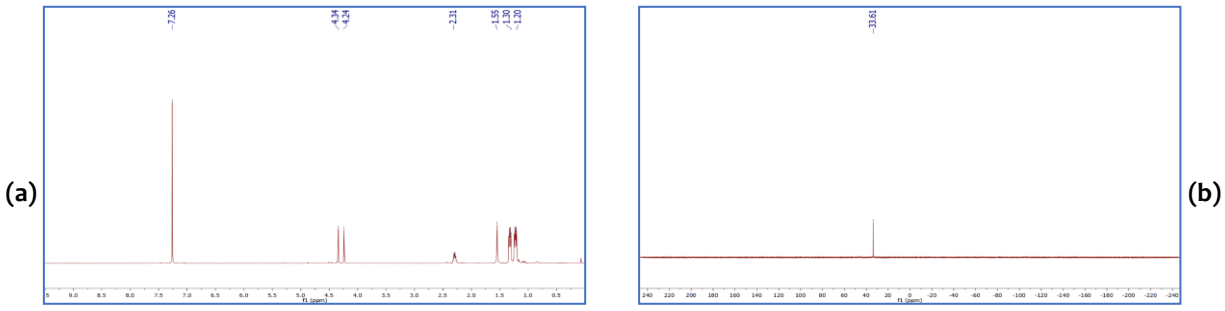


Fig. 2(a).3.8 (a) ^{1}H NMR Spectrum, **(b)** ^{31}P Spectrum for **C-8** complex.

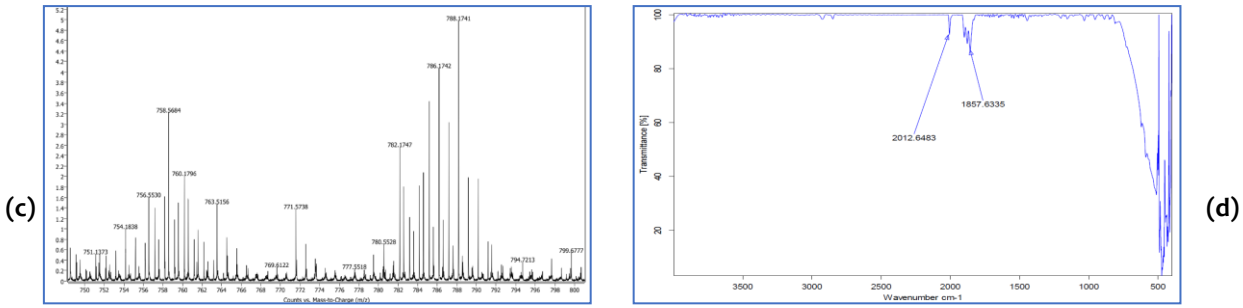
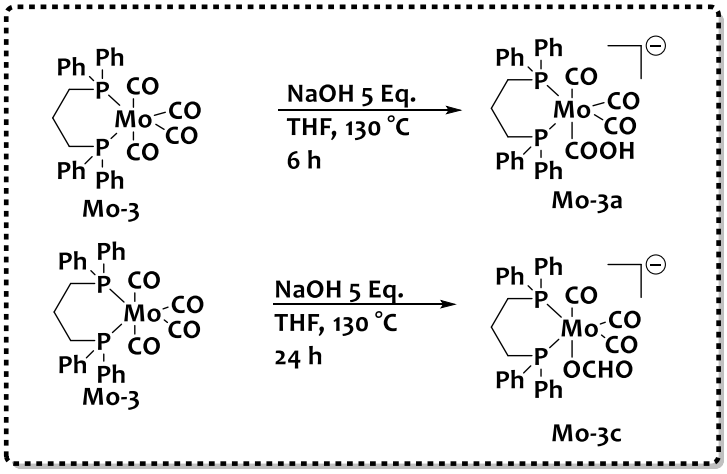


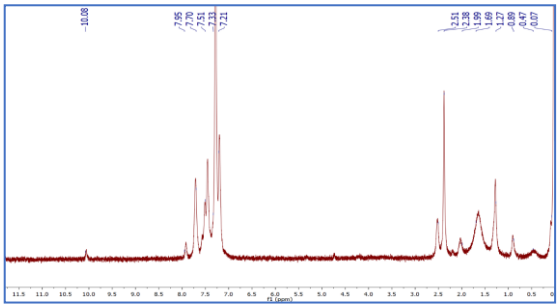
Fig. 2(a).3.8 (c) ESI-MS Spectrum, **(d)** FTIR Spectrum for **C-8** complex.

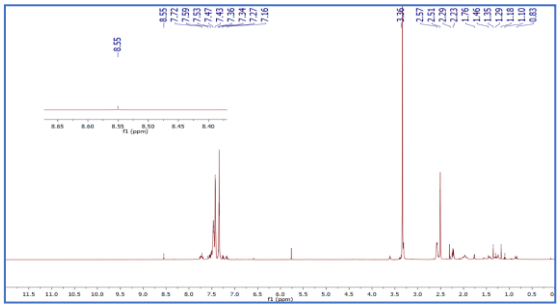
2(a).3.9 Mechanistic Experiments



Scheme 2(a).2 Scheme for mechanistic experiments.

(a)





(b)

Fig. 2(a).3.9 (a) ^{1}H NMR for carboxylic intermediate **C-3a, (b)** ^{1}H NMR for formate intermediate **C-3c** complex.

2(*b*)

Bench-Stable Low-Valent Chromium Catalysts for Hydrogenation of CO_2, Bicarbonate and Inorganic Carbonates to Formate

Research Article based on this study:
Singh, T.; Gutal, A.; Regina, A.; Banerjee, A.; Paranjothy, M.; Chakraborty, S. Bench-Stable Low-Valent Chromium Catalysts for Hydrogenation of CO_2, Bicarbonate, and Inorganic Carbonates to Formate. *ACS Catal.* **2024**, 14958-14965.

2(b).1. Introduction

Carbon dioxide comprises one of the major greenhouse gases released in the biosphere resulting from fossil fuel depletion. The increase in CO_2 concentration in the atmosphere since industrial revolution is presently a major concern leading to unusual climate changes and global warming.[15] CO_2 has the potential to serve as an attractive, renewable and cost-effective feedstock for the manufacture of numerous fine and bulk chemicals. CO_2 is nontoxic, naturally abundant, economical, and valuable alternative to commercially applied noxious chemicals like CO and phosgene etc.[23] Furthermore, utilization of CO_2 as a C1 scaffold to produce value-added chemicals and energy carriers paves the way for an effective circular economic model.[24] In this context, catalytic hydrogenation of CO_2 to formic acid/formate is a highly desirable process in comparison to existing routes and in view of closed-cycle economy.[29,71] Formic acid is an essential chemical used in silage production for animal feed, leather and textile industries for tanning and dyeing, as reducing agent, and for the production of varnishes, plasticizers, resins, and glass.[143] Formic acid is also perceived to be used directly as fuels or to generate H_2 on demand, rendering it as an attractive hydrogen carrier.[144-145] However, activation of CO_2 is problematic because of thermodynamic stability and kinetic inertness. Moreover, the formation of formic acid from the reaction of CO_2 and H_2 is an endergonic process ($\Delta G°_{298}$ = +32.8 kJ mol^{-1}) owing to unfavorable entropy conditions.[82] Hence commonly a base is used to drive the reaction towards product formation making the overall process thermodynamically downhill. Despite these challenges, advancement on homogeneous CO_2 hydrogenation to formic acid/formate using well-defined transition metal-based complexes is noteworthy.[28,38,39,219] Since the seminal work by Inoue et al. in 1976,[81] a large number of homogeneous catalysts have been discovered for the hydrogenation of CO_2 to formic acid/formate exhibiting remarkable catalytic activities.[37,49,77,133,204,220,221] In 2009 Nozaki group demonstrated pincer PNP ligand-based iridium(III) catalyzed hydrogenation of CO_2 achieving highest TON of 3,500,000 for the formate formation.[205] Nevertheless, the majority of the homogeneous catalysts reported are derived from noble precious metals. High cost, low earth-abundancy and toxicity issues of platinum group metal complexes prompted scientific community to delve into earth-abundant, low-toxicity, non-precious 1st row transition metal-based complexes in executing the targeted task.[50,52] Indeed, notable research advancement have been made in exploiting first-row base metals in homogeneous catalysis.[51,53,55-57] Significant development on carbon dioxide hydrogenation to formic acid/formate catalyzed by complexes of Fe, Co, Ni, Cu, Mn have also been accomplished triggered by the groups of Beller, Milstein and others.[58,86-88,92,95,100-102,105-107,111-113,116,117,119,121,122,124,126,202,222,223] Selected noteworthy examples are shown in Figure 2(b).1 Klankermayer described CO_2 hydrogenation with the catalyst formed by the composition of $Ni(BF_4)_2.6H_2O$ & NP_3 producing formate with a very high TON of 4,650,000.[124] Lately, a Mn pincer complex bearing triazine backbone was developed by Beller group for the hydrogenation

of CO_2 to formate and a total TON of 2,000,000 was reported (Figure 2(b).1).[126] Bidentate phosphine based non-pincer complexes of Co, Ni and Mn were also discovered for CO_2 hydrogenation. In 2014 Linehan reported DMPE-based cobalt hydride complex as an active catalyst in the CO_2 hydrogenation.[102] In 2017 they also revealed a nickel bis-phosphine catalyzed CO_2 hydrogenation.[111] Kirchner and Gonsalvi disclosed CO_2 hydrogenation utilizing bench-stable, Large wide bite angle supported Mn complex as catalyst.[124] We have recently reviewed progress on base metal catalyzed CO_2 hydrogenation to formate.[202]

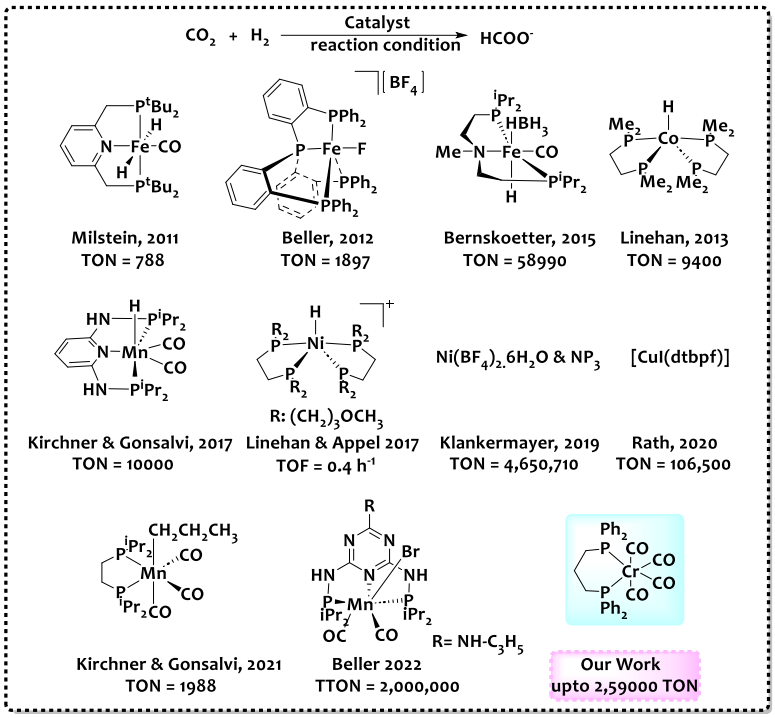


Fig. 2(b).1 Selected base metal catalysts reported for CO_2 hydrogenation to formate.

Despite landmark discoveries on 3d metal catalyzed homogeneous reactions, to our surprise utilization of earth-abundant, inexpensive chromium complexes in homogeneous (de)hydrogenation reactions remained underdeveloped.[222-230] Lately, well-defined Cr complexes have been used in dehydrogenative coupling reactions such as N-Alkylation of amines via borrowing hydrogen strategy, dehydrogenative coupling of alcohols and amines, β-alkylation of secondary alcohols by the groups of Kempe and others.[222-226] Hydrogenation reactions using Cr carbonyl complexes dates back to late 1960s with the application of arenetricarbonylchromium complexes for C=C hydrogenation.[227] Hydrogenation of ketones, aldehydes, polycyclic aromatic hydrocarbons as well as the semi hydrogenation of alkynes were also reported catalyzed by chromium complexes subsequently.[227-231, 131] Recently, Gudat group employed N-heterocyclic phosphenium ligand supported chromium complex for the transfer hydrogenation of CO_2 to formate and methanol in the presence of ammonia borane.[233]

Decades back Darensbourg and coworkers probed hydrogenation of carbon dioxide to alkyl formate catalyzed by anionic chromium hydridocarbonyl complex in alcoholic solvent albeit very low TON of 14.6. Prompted by this state-of-the-art discovery on CO_2 hydrogenation and recent development on cobalt, nickel and manganese complexes bearing bidentate phosphine ligands[102,111,122] catalyzed hydrogenation of CO_2, we were intrigued to explore catalytic performance of low-valent chromium carbonyl complexes coupled with diphosphine ligands. Bidentate phosphine ligands display unique characteristic in terms of electronics by their donicity, and in size by their steric bulk (bite angle).[206,234,235] Herein, we report highly efficient chromium catalysts bearing natural bite angle bidentate phosphine ligands for hydrogenation of CO_2, biologically relevant $NaHCO_3$ and inorganic carbonates to formate.

2(b).2 Methods

At the outset catalytic activities of preformed complexes of $Cr(CO)_6$ with several small, natural and large bite angle-based bidentate phosphine ligands (**C-1**-**C-6**) were investigated in the hydrogenation of carbon dioxide. Cr (DPPM)$(CO)_4$ (DPPM=1,1Bis(diphenylphosphino)methane) (**C-1**), Cr(DPPE)$(CO)_4$ (**C-2**; DPPE=1,2 Bis(diphenylphosphino)ethane), Cr(DPPP)$(CO)_4$ (DPPP=1,3-Bis(diphenylphosphino)propane)(**C-3**), and Cr(DPPF)$(CO)_4$ (**C-4**; DPPF = 1,1′-Bis(diphenylphosphino)ferrocene) were prepared according to literature procedures.[236,237] Initially 2.6 μmol of small bite angle DPPM-based **C-1** was used for CO_2 hydrogenation in the presence of NaOH at 130 °C in THF/H_2O solvent mixture and a total of 40 bar (CO_2: H_2 = 1:3)

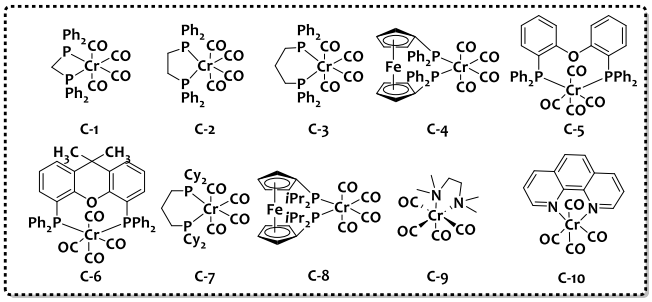
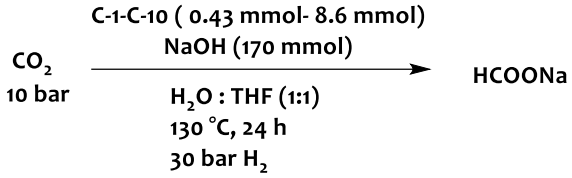


Fig. 2(b).2 Chromium complexes tested for CO_2 hydrogenation.

pressure, which resulted in a TON of 36,395 (Table 2(b).1, entry 1). When **C-2** (1.7 μmol) was used as catalyst, formate was obtained with a TON of 32,630 under identical condition (Table 2(b).1, entry 2). To our delight, well-defined Cr(DPPP)$(CO)_4$ **C-3** (0.43 μmol) yielded formate in decent yield (60%) corresponding to a maximum TON of upto 259,000 (Table 2(b).1, entry 3). Large bite angle DPPF-based complex **C-4** (1.8 μmol) and newly prepared novel complexes Cr(Dpephos)$(CO)_4$ (**C-5**) (1.4 μmol) Cr(Xanthphos)$(CO)_4$ (**C-6**) (1.3 μmol) (Figure 2) were also explored in the hydrogenation of CO_2 exhibiting inferior catalytic activities under the optimum reaction conditions in comparison to **C-3** (Table 2(b).1, entries 4-6). Hence bite angle of the ligands plays a prominent role in determining the catalytic performance of the complexes. A catalytic reaction was also conducted using $Cr(CO)_6$ in the absence of phosphine ligand resulting in a TON of 18,490 in the presence of NaOH base after 24 h at 130 °C (Table 2(b).1, entry 7) indicating the vital role of phosphine ligands in obtaining higher yields of desired product. As anticipated trace amount of product was obtained performing reaction in absence of catalyst Table 2(b).1, entry 8). The influence of ligand electronics on the catalytic activity was also investigated. Accordingly, a novel 1,3 Bis(dicyclohexylphosphino) propane (DCYPP) ligand supported chromium complex Cr(DCYPP)$(CO)_4$ **C-7** was synthesized (Scheme 2(b).2) and explored in the CO_2 hydrogenation. 0.41 μmol **C-7** furnished formate with a TON of 96900 (Table 2(b).1, entry 9). Literature known complex[210] Cr(Dippf)$(CO)_4$ (DiPPF= 1,1′-Bis(diisopropylphosphino)ferrocene), 1.63 μmol) **C-8** displayed a formate TON of 34,190 (Table 2(b).1, entry 10). So natural bite angle based DPPP ligand (91°) supported complex **C-3** was found to be an efficient catalyst among the bisphosphine ligand-derived catalysts examined. A graph for the plot of the bite angle *vs* TOF for the **C-1** to **C-6** is shown in Figure 2(b).3 . Moreover, two nitrogen-based tetracarbonyl complexes were also synthesized[211,238] using literature protocols and screened in CO_2 hydrogenation (Figure 2(b).2). Exploring 8.6 μmol Cr(TMEDA)$(CO)_4$ (TMEDA= tetramethylethylenediamine) **C-9** yielded formate with a TON of 1125 (Table 2(b).1, entry 11). Upon utilizing 5.5 μmol Cr(1,10 phenanthroline)$(CO)_4$ **C-10**, a formate TON of 6150 was recorded (Table 2(b).1, entry 12). Screening different bases like Et_3N, Na_2CO_3, and DBU was also carried out for optimum catalytic activities. We could detect only trace amount of respective formate products in each case (Table 2(b).1, entries 13-15). Nevertheless, when TMNO or NaOH were used as additives TONs of 3132 and 7714 were recorded, respectively for the production of formate in the presence of 10 mmol DBU (Table

2(b).1, entries 16-17). K_3PO_4 (30 mmol) and K_2CO_3 (30 mmol) were also assessed giving formate with TONs of 1440 and 905, respectively (Table 2(b).1, entries 18-19).

Table2(b).1 Chromium catalyzed CO_2 hydrogenation to formate.[a]



Entry	Base	Catalyst	Pressure(CO_2:H_2)	Solvent	TON[b,c]
1	NaOH	**C-1**	10:30	THF:H_2O	36,395
2	NaOH	**C-2**	10:30	THF:H_2O	32,630
3	NaOH	**C-3**	10:30	THF:H_2O	259,000
4	NaOH	**C-4**	10:30	THF:H_2O	55,555
5	NaOH	**C-5**	10:30	THF:H_2O	58,500
6	NaOH	**C-6**	10:30	THF:H_2O	45,560
7	NaOH	$Cr(CO)_6$	10:30	THF:H_2O	18,490
8	NaOH	-	10:30	THF:H_2O	Trace
9	NaOH	**C-7**	10:30	THF:H_2O	96,900
10	NaOH	**C-8**	10:30	THF:H_2O	34,190
11	NaOH	**C-9**	10:30	THF:H_2O	1,125
12	NaOH	**C-10**	10:30	THF:H_2O	6,150
13[d]	Et_3N	**C-3**	10:30	THF:H_2O	Trace
14[e]	Na_2CO_3	**C-3**	10:30	THF:H_2O	Trace
15[f]	DBU	**C-3**	10:30	THF:H_2O	Trace
16[g]	DBU	**C-3**	10:30	THF:H_2O	3,130
17[h]	DBU	**C-3**	10:30	THF:H_2O	7,715
18[i]	K_3PO_4	**C-3**	10:30	THF:H_2O	1,440
19[j]	K_2CO_3	**C-3**	10:30	THF:H_2O	905

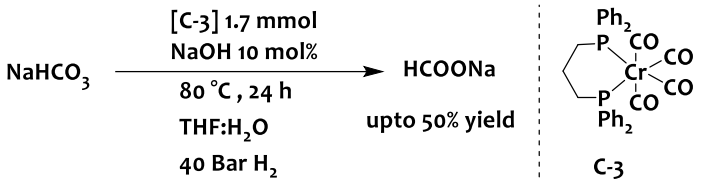
20[k]	KOH	**C-3**	10:30	THF:H_2O	2,185
21[l]	^{t}BuOK	**C-3**	10:30	THF:H_2O	19,160
22	^{t}BuOK	**-**	10:30	THF:H_2O	Trace
23	NaOH	**C-3**	10:30	H_2O	46,185
24	NaOH	**C-3**	10:30	THF	5,070
25	NaOH	**C-3**	10:30	DMSO:H_2O	171,070
26	NaOH	**C-3**	10:10	THF:H_2O	119,580
27[m]	NaOH	**C-3**	10:30	THF:H_2O	71,650

[a]Reaction conditions: Unless and otherwise stated 130 °C, 30 bar H_2 at room temperature, 10 bar CO_2, 24 h, 170 mmol NaOH, certain mmol catalyst. [b]Yield based on ^{1}H NMR signals of sodium formate, with DMF used as an internal standard. [c]Turnover number = moles of sodium formate per mole of catalyst. [d]50 mmol Et_3N was used. [e]50 mmol Na_2CO_3 was used. [f]45 mmol DBU was used. [g]0.1 mmol TMNO was taken along with 10 mmol DBU, 0.14 µmol C-3 was taken. [h]0.1 mmol NaOH was taken along with 10 mmol DBU, 0.14 µmol C-3 was taken. [i]30 mmol K_3PO_4 was taken. [j]30 mmol K_2CO_3 was taken. [k]50 mmol KOH was taken. [l]100 mmol ^{t}BuOK was taken.[m]100 mmol NaOH was taken.

However, in case of KOH (50 mmol), a lower TON of 2185 for the corresponding formate (Table 2(b).1, entry 20) was observed. Pleasingly, when 100 mmol ^{t}BuOK was explored as base under optimized conditions, formate TON escalated to 19,160 (Table 2(b).1, entry 21). Thus, it is obvious that the nature of base and high basic reaction media played a critical role in obtaining higher yield of the desired formate. Trace amount of formate was obtained as product when reaction was carried out in presence of ^{t}BuOK but without catalyst (table 2(b).1, entry 22). Surprisingly, TON decreased to 46,185 when reaction was performed in only water media (Table 2(b).1, entry 23), whereas a very low TON of 5070 was obtained by carrying out the reaction in THF (Table 2(b).1, entry 24). DMSO/H_2O combination gave high TON of 171,070 under the optimized reaction conditions (Table 2(b).1, entry 25). Lowering the gaseous pressure to 20 bar (CO_2: H_2 =10:10), a TON of 119,580 was achieved (Table 2(b).1, entry 26). Performing the reaction with 100 mmol NaOH under optimum conditions furnished formate with a TON of 71,650 (Table 2(b).1, entry 27). Notably, the catalyst is air-stable displaying no changes in the ^{31}P NMR leaving the catalysts under open air up to several weeks. A recyclability test was also performed by separating the organic layer out of biphasic reaction mixture obtained after completion of the reaction. The catalytic activity of **C-3** was retained upto 55% in subsequent step.

We were also curious to probe the catalytic performance of **C-3** in sodium bicarbonate and inorganic carbonate hydrogenation. Much less work on the biologically relevant reduction of carbonates and bicarbonates have been reported,[86,101] and the activities of those hydrogenation catalysts are significantly lower in comparison to the reaction of CO_2. Excitingly, a loading of 1.7 µmol **C-3** in conjunction with 10 mol% NaOH, 40 bar H_2 at 80 °C in THF/H_2O mixture hydrogenated sodium bicarbonate to sodium formate with 50% yield after 24 h (Table 2(b).2, entry 1). Upon increasing the H_2 pressure to 60 bar the yield of formate was decreased to 23% (Table 2(b).2, entry 2). However, when ^{t}BuOK was used as base, the yield decreased to 22% (Table 2(b).2, entry 3). Carrying out the reaction in the absence of NaOH, only 3% yield was recorded as shown by NMR spectra (Table 2(b).2, entry 4). Trace amount of product could be detected when reaction was performed without catalyst (Table 2(b). 2, entry 5).

Table2(b).2 Chromium catalyzed hydrogenation of sodium bicarbonate.[a]

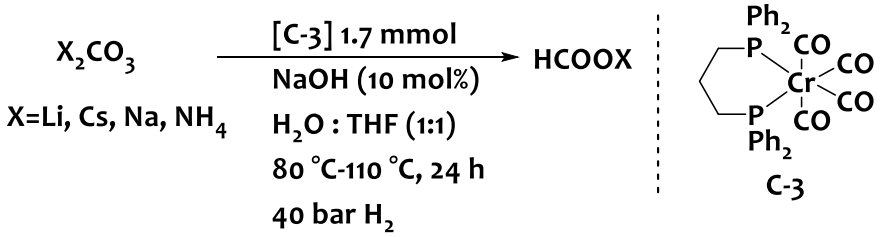


Entry	Base	Catalyst	Pressure	Solvent	Yield[b]
1	NaOH	**C-3**	40	THF:H_2O	50%
2	NaOH	**C-3**	60	THF:H_2O	23%
3	*t*-BuOK	**C-3**	40	THF:H_2O	22%
4	-	**C-3**	40	THF:H_2O	3%
5	-	-	40	THF:H_2O	0%

[a]Reaction conditions: $NaHCO_3$ 0.5 mmol, 80 °C, 40 bar H_2, 24 h,1.7 µmol catalyst (**C-3**), 10 mol% NaOH.
[b]Yield based on ^1H NMR signals of sodium formate with DMF used as an internal standard.

C-3 was also explored in the hydrogenation of inorganic carbonates. Lithium carbonate was taken as the benchmark substrate. Interestingly, an exquisite yield of 56% for the formate formation was achieved using 1.7 µmol **C-3** in the presence of 10 mol% NaOH in THF/H_2O mixture at 110 °C after 24 h applying 40 bar H_2 pressure (Table 2(b).3, entry 1). However, in case of caesium carbonate the desired product was obtained in very low yield (9%; Table 2(b).3, entry 2). No product formation was observed when ammonium carbonate was used as carbonate surrogate as indicated by NMR (Table 2(b).3, entry 3). Sodium carbonate was hydrogenated to formate in 6% yield as revealed by NMR spectra (Table 2(b).3, entry 4). In order to get insights into the reaction mechanism of CO_2 hydrogenation, **C-3** was probed for stochiometric experiments. Initially a THF solution of **C-3** was heated overnight at 130 °C for 12 h. However, no change was observed in the ^{31}P and IR spectroscopy. Then 5 equiv. of NaOH was added to a THF solution of **C-3** and kept for heating at 130 °C. The ^{31}P NMR spectrum after 1 h revealed appearance of a new signal at 32.1 ppm along with the peak at 42 ppm for starting material **C-3** indicating the formation of a new complex. The ^{31}P NMR signal of **C-3** disappeared heating the reaction mixture for longer period of time (figure 2(b).3.11(b)).

Table2(b).3 Chromium catalyzed inorganic carbonate hydrogenation.[a]

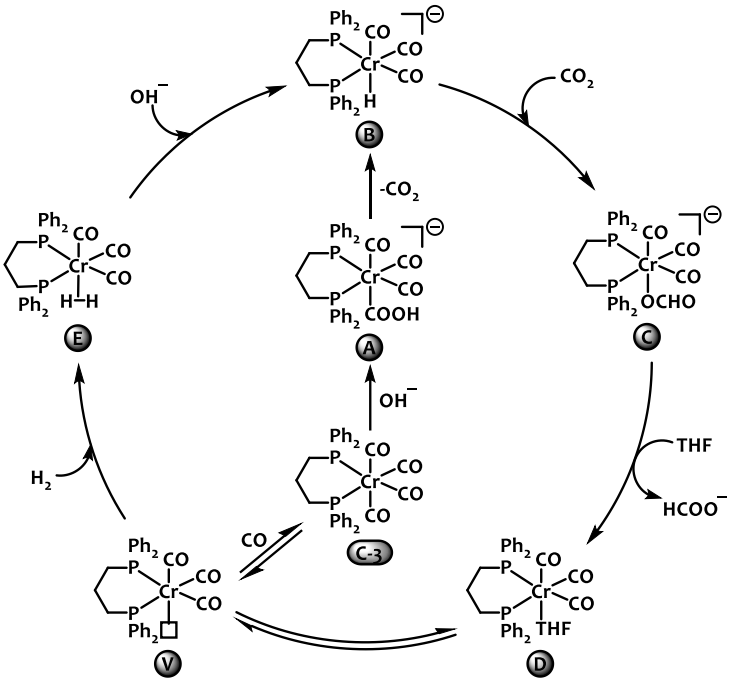


Entry	Base	Catalyst	Solvent	Yield[b]	X
1[c]	NaOH	**C-3**	THF:H_2O	56%	Li
2	NaOH	**C-3**	THF:H_2O	9%	Cs
3	NaOH	**C-3**	THF:H_2O	0%	NH_4
4	NaOH	**C-3**	THF:H_2O	6%	Na

[a]Reaction conditions: X2CO3 (X= Li, Cs, Na, NH4) 0.5 mmol, 80 °C, 40 bar H_2 at room temperature, 24 h, 1.7 µmol catalyst (C-3), 10 mol% NaOH. [b]Yield based on ^{1}H NMR signals of sodium formate, with DMF used as an internal standard. [c]110 °C temperature.

In the ^{1}H NMR spectrum, a new signal at 10.2 ppm in $CDCl_3$ was observed, which disappeared in D_2O owing to the exchange of the proton with deuterium. The aforementioned spectroscopic data supported formation of an anionic metallacarboxylate complex A (Scheme 2(b).2)[214-216] The formation of a metallacarboxylate **A** was further confirmed by IR spectroscopy exhibiting a ν_{CO} signal of the carboxylate at 1598 cm^{-1}, which is in line with the simulated spectra. The ^{13}C{^{1}H} NMR spectra displayed a signal at 178 ppm corresponding to the metal attached carboxylate carbon. Further heating the reaction mixture revealed appearance of a peak at 8.3 ppm in the ^{1}H NMR spectrum and a signal at 170 ppm in the ^{13}C NMR spectrum . This newly formed compound is assigned as the formato complex **C** (Scheme 2(b).1). In the IR spectroscopy a strong ν_{CO} at 1651 cm-1 was observed assigned for the formate stretching vibration. The complex was also identified in the HRMS study. However, there was no significant changes in the ^{31}P NMR spectrum in comparison to **A**. Conversion of carboxylate to formate is expected to proceed via intermediate hydride complex **B** (Scheme 2(b).1). Attempts to characterize the hydride complex B by NMR spectroscopy failed probably owing to conversion of **B** to **C** or poor solubility under the reaction condition. Formation of an anionic hydride bridged complex [µ-HCr(CO)$_6$(DPPP)$_2$]- from **B** cannot be completely excluded at this stage.[128]

Kinetic isotopic experiments were also carried out by correlating the reaction rates in H_2O:THF and D_2O:THF in independent experiments. Initially, a reaction was performed with C-3, 5 mmol NaOH and 20 bar total pressure (H_2: CO_2= 15:5) for 36 h resulting in formate TON of 2265, which was taken as benchmark reaction for rate comparison. When the hydrogenation reaction was performed under similar condition in D_2O:THF mixture with H_2:CO_2 (in 15:5 ratio), formate was obtained in lower yield as revealed by ^{1}H NMR spectrum. However, there was no deuterium peak corresponding to DCOONa as revealed by ^{2}H NMR indicating absence of H/D exchange in D_2O solvent. Solvent KIE (H_2O/H_2-D_2O/H_2) value ([rate in H_2O]/[rate in D_2O]) in this case was calculated to be 8.81. Additionally, when D_2 was taken in place of H_2, DCOONa was the only product obtained when analyzed using ^{1}H and ^{2}H NMR, which was further quantified using HPLC.[239] The KIE value ([rate with H_2]/ [rate with D_2] in H_2O/THF mixture was calculated to be 9.74 in this case. DCOONa was also detected using D_2 as fed gas and D_2O:THF as solvent. A high experimental k_H/k_D value suggests that proton transfer and hydride transfer steps play important roles in important determining the rate of the overall reactions. As per the theoretical calculation, hydride transfer has a barrier and the existence of a finite barrier for the hydride transfer step results in a higher KIE value in the case of the D_2/H_2O reaction. However, proton transfer is a barrierless reaction that necessitates variational treatment for rate constant calculation. Moreover, upon semi-classical calculation of theoretical k_H/k_D value for the hydride transfer step, we found it to be close to unity, suggesting quantum tunnelling effect play a crucial role in the experiment. In a related study on Ir catalyzed CO_2 hydrogenation by Cheng, Wang, Lin and coworkers found calculated H/D KIE to be also small.[239] Nevertheless, these KIE's are not derived from measuring actual rate constants and several equilibrium isotope effect might also be involved.[34b] Thus, the observed experimental and theoretical data avoid the unambiguous implication that the rate limiting step involves X-H bond formation/breakage.



Scheme 2(b).1 Proposed mechanism for Cr-3 catalyzed CO_2 hydrogenation.

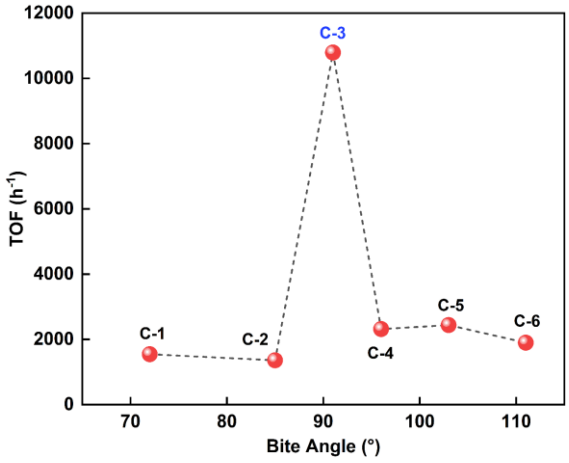


Fig. 2(b).3 Plot of Bite Angles of complexes VS TOF(h^{-1}).

To corroborate our experimental findings theoretical calculations were performed using M06L/6-311++G**[SDD/ECP(Cr)][240] level of theory with ORCA -5.0 software package.[241]Atomicity of both the mechanisms were kept constant (for details see supplementary information). Solvent effects (THF) have been included using the conductor-like polarizable continuum model (CPCM).[242] Vibrational normal modes and harmonic frequencies for stationary structures were obtained through the diagonalization of the ground state energy second derivative matrix. Harmonic vibrational frequencies were calculated to confirm the local minimum energy structures. Zero-point energy and thermal corrections have been included in our reaction free energy calculations under T = 298.15 K and 1 atm pressure conditions Harmonic vibrational frequencies were calculated to characterize the nature of stationary points. Transition states (TSs) were characterized due to the presence of an imaginary vibrational frequency. The climbing-image variant of NEB (CI-NEB) method in ORCA was used to find the TS with convergence tolerances for climbing image ("saddle-point") Max(|F|): 5.00E-4 Eh/Bohr and RMS(F): 2.50E-4 Eh/Bohr. The Gibbs free energy profile for two possible reaction pathways M1 and M2 presented in Figure 3 was generated using M06L/6-311++G**[

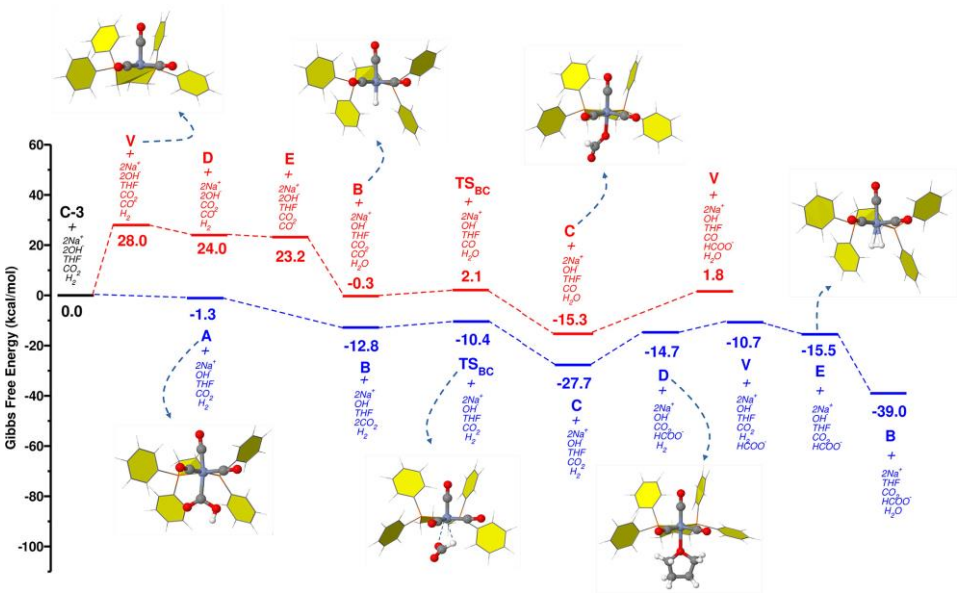


Figure 2(b).4 Gibbs energy profile (in Kcal/mol) of the possible reaction pathways, M1 (blue) and M2 (red) using M06L/6-311++G**[SDD/ECP(Cr)] level of theory. THF is used as solvent using CPCM solvation model.

SDD/ECP(Cr)] level of theory. Theoretical studies for pathway **M1** in Figure 2(b).4 revealed that metallacarboxylate **A** is lower in energy (-1.3 kcal/mole) with respect to the starting complex **C-3** (Scheme 2(b).1). Further, hydride **B** turned out to be of lower in energy by 11.5 kcal/mole with respect to **A**. Formato complex **C** was formed by insertion of CO_2 into M-H bond of **B** via TSBC with an activation barrier of 2.4 kcal/mol and **C** was found to be thermodynamically more stable by -14.9 kcal/mol under the reaction conditions with respect to **B**. Therefore, reversible isomeric transformation of metallacarboxylate and formato complex seems impossible and the conversion is expected to undergo via hydride intermediate **B**. Further release of HCOO- and concomitant formation of THF complex **D** is lower in energy by 1.9 kcal/mol with respect to **B**. Alternatively, elimination of a CO molecule from **C-3** can generate a coordinatively unsaturated complex **V**, which is unstable with respect to **C-3** by 28.0 kcal/mol in the second possible pathway (**M2**, Figure 2(b).4). However, subsequent steps for pathway M2 are exergonic in nature with respect to V but similar topology of surface is seen for **M2-B→M2-TSBC→M2-C** region with elevated free energies hence this pathway seemed less plausible.

Based upon the experimental findings along with theoretical investigation we discerned that initial nucleophilic attack of OH^- onto one of the CO of **C-3** generates metallacarboxylate species **A**. Subsequent evolution of CO_2 from **A** furnished the hydride complex **B**, which is expected to be the key species of the catalytic cycle. Insertion of CO_2 into the metal-hydride bond of **B** afforded the thermodynamically stable formato complex **C**. Base assisted release of formate from **C** formed the THF complex **D**, which on reaction with H_2 gave a sigma complex **E** via unsaturated species V. Finally, **E** in presence of NaOH deprotonates the coordinated H_2 ligand from **E** regenerating the hydride **B** and completes the catalytic cycle (Scheme 2(b).1).

2(b).3 Experimental Section

Complexes (**Cr-1**, **Cr-2**, **Cr-3**, **Cr-4**, **Cr-8**, **Cr-9**, **Cr-10**) were synthesized by charging the Schlenk flask with $Cr(CO)_6$ and toluene solution of respective phosphine, nitrogen based ligands in equimolar ratio inside the glove box. Reaction mixture was heated at 120 °C for 48 hours. Afterwards, reaction was stopped, cooled and solvent was dried under vacuum, and the obtained data was as par with the available data.[211,236-238] **Cr-5** to **Cr-7** were prepared as per the Scheme 2(b).2.

2(b).3.1 Representative Characterization Data for Complex C-1

$CrDPPM(CO)_4$ (**C-1**)
^{1}H NMR (500 MHz, $CDCl_3$) δ 7.45-7.19m(Ar), 4.38(t).
$^{31}P\{^1H\}$-NMR (203.0 MHz, $CDCl_3$) δ 26.23 (s, 2P).

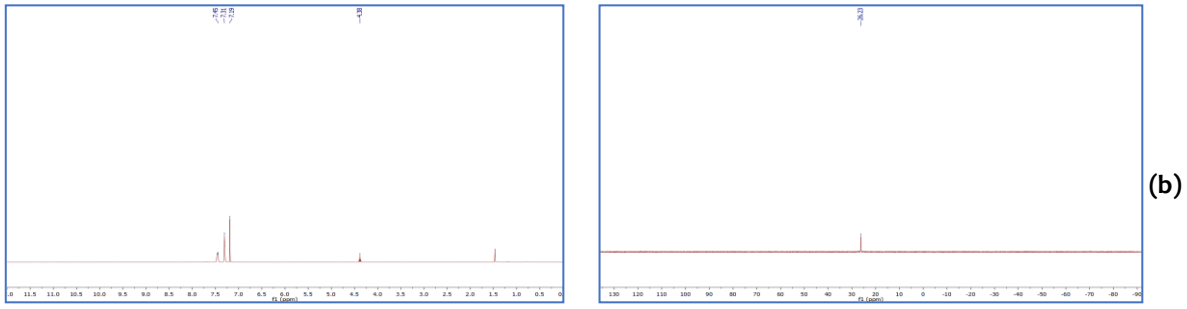


Fig. 2(b).3.1 (a) ^{1}H NMR Spectrum, **(b)** ^{31}P Spectrum for **C-1** complex.

2(b).3.2 Representative Characterization Data for Complex C-2

$CrDPPE(CO)_4$ (**C-2**)
^{1}H NMR (500 MHz, $CDCl_3$) δ 7.60-7.37 m(Ar), 2.59 m(2H), 2.55 m(2H).
$^{31}P\{^1H\}$-NMR (203.0 MHz, $CDCl_3$) δ 80.5 (2P).

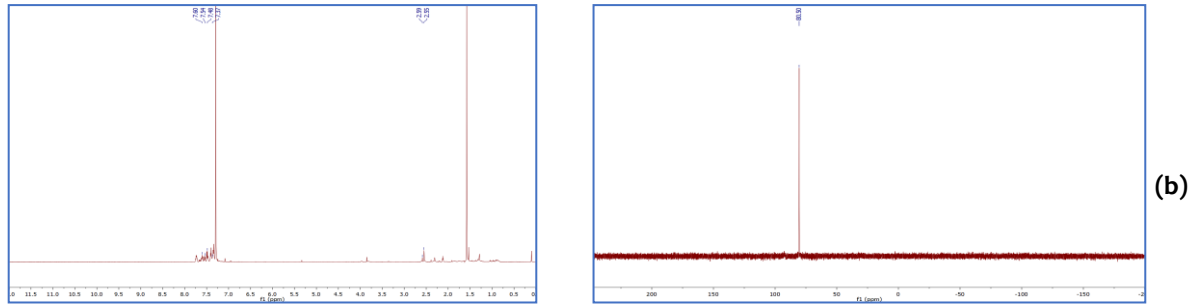


Fig. 2(b).3.2 (a) ^{1}H NMR Spectrum, **(b)** ^{31}P Spectrum for **C-2** complex.

2(b).3.3 Representative Characterization Data for Complex C-3

$CrDPPP(CO)_4$ (**C-3**)
^{1}H NMR (500 MHz, $CDCl_3$) δ 7.44-7.26 m(Ar), 2.44m(4H), 1.97(2H).
$^{31}P\{^1H\}$-NMR (203.0 MHz, $CDCl_3$) δ 42.36 (2P).

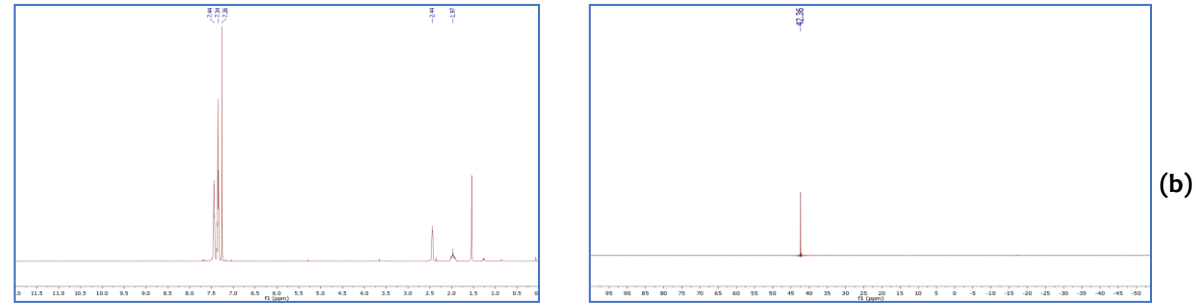


Fig. 2(b).3.3 (a) ^{1}H NMR Spectrum, **(b)** ^{31}P Spectrum for **C-3** complex.

2(b).3.4 Representative Characterization Data for Complex C-4

$CrDPPF(CO)_4$ (**C-4**)
^{1}H NMR (500 MHz, $CDCl_3$) δ 7.26-7.60 m(Ar), 4.25m (8H).

$^{31}P\{^{1}H\}$-NMR (203.0 MHz, $CDCl_3$) δ 51.70(2P).

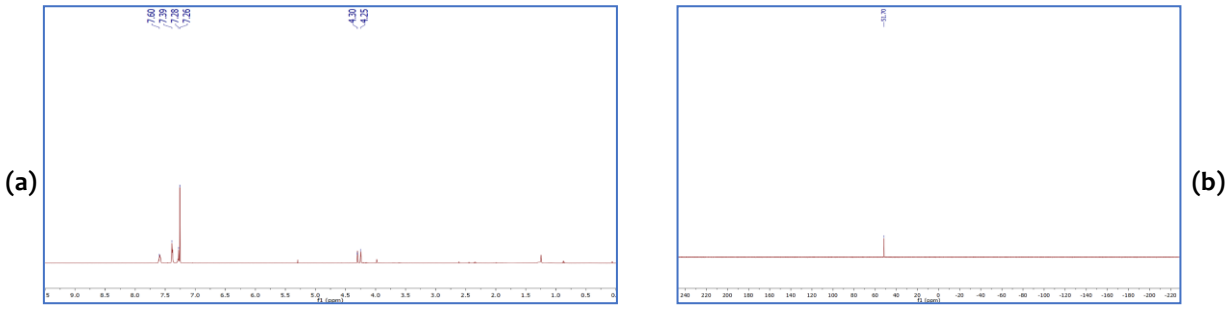
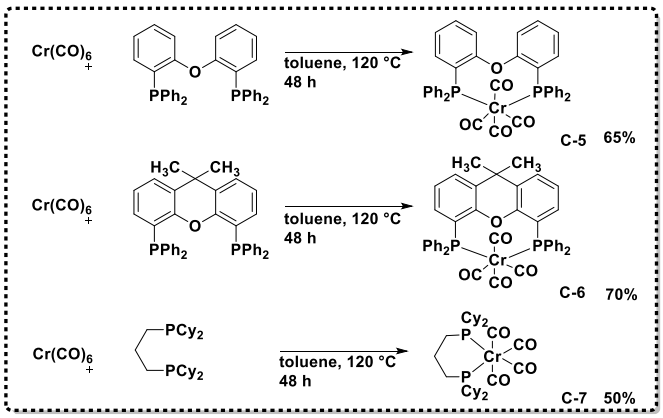


Fig. 2(b).3.4 (a) ^{1}H NMR Spectrum, **(b)** ^{31}P Spectrum for **C-4** complex.



Scheme 2(b).2 Scheme for the synthesis of complexes **C-5** to **C-7** .

2(b).3.5 Representative Characterization Data for Complex C-5

Cr $(CO)_6$ (0.1320 g, 0.6mmol) was added to an oven dried Schlenk tube already charged with 4ml Toluene solution of DPEPHOS (0.2692 g, 0.5 mmol) inside the glove box. Schleck was taken out of the glove box and placed in a pre-heated oil bath at 120 °C for 48 hours. Afterwards the reaction was stopped and allowed to cool at room temperature, greenish solution was obtained which was filtered and dried under vacuum. Resulted residue was washed with pentane twice and dried overnight, green powder was obtained (65%) yield. Single crystals suitable for diffraction were obtained by diffusing hexane in saturated DCM solution of compound.

^{1}H NMR (500 MHz, $CDCl_3$) δ 7.67(2H, d), 7.43-7.10(20H), 6.98(2H, t).
^{13}C NMR (126 MHz, $CDCl_3$) δ 226.38 (m), 221.60 (t), 135.14 (m), 133.36 (t), 133.11, 131.29, 129.29, 128.14 (t), 127.36 (m), 125.33, 124.16, 120.45.
^{31}P NMR (203 MHz, $CDCl_3$) δ 47.49.
FT-IR cm^{-1} 2006 (CO), 1911 (CO), 1862(CO).

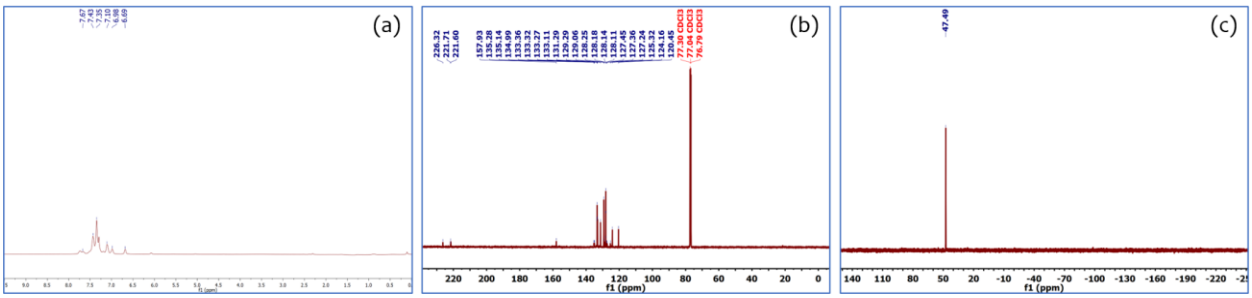
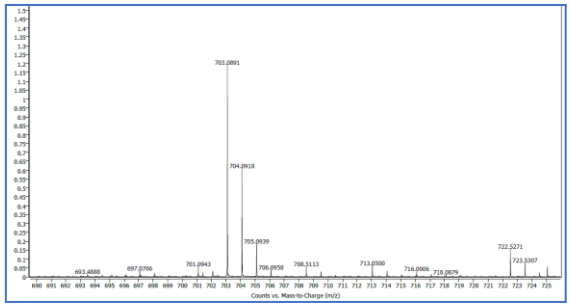
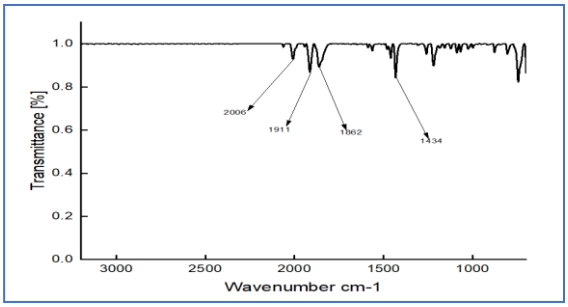


Fig. 2(b).3.5 (a) ^{1}H NMR Spectrum, **(b)** ^{13}C Spectrum, **(c)** ^{31}P Spectrum for **C-5** complex.

(d)





(e)

Fig. 2(b).3.5 (d) ESI-MS Spectrum, **(e)** FTIR Spectrum for **C-5** complex.

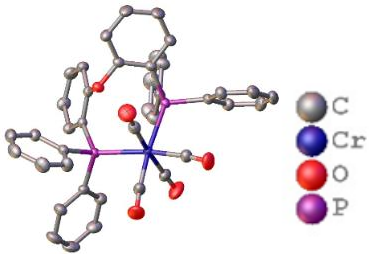


Fig. 2(b).3.5 (f) ORTEP Drawing of **C-5** complex.

Table 2(b).4 Crystal data and structure refinement for **C-5.**

CCDC no.	2312962
Empirical formula	$C_{40}H_{28}CrO_5P_2$
Formula weight	702.56
Temperature/K	297.0
Crystal system	triclinic
Space group	P-1
a/Å	9.4321(11)
b/Å	13.6037(16)
c/Å	13.8526(16)
α/°	74.914(3)
β/°	81.728(3)
γ/°	82.599(3)
Volume/Å3	1690.6(3)
Z	2
ρcalcg/cm3	1.380
μ/mm-1	0.478
F(000)	724.0
Crystal size/mm3	0.2 × 0.15 × 0.11
Radiation	MoKα (λ = 0.71073)
2Θ range for data collection	3.114 to 50.04
Index ranges	-11 ≤ h ≤ 11, -16 ≤ k ≤ 16, -16 ≤ l ≤ 16
Reflections collected	39760
Independent reflections	5908 [Rint = 0.0266, Rsigma = 0.0168]
Data/restraints/parameters	5908/0/433
Goodness-of-fit on F2	1.030
Final R indexes [I>=2σ (I)]	R1 = 0.0300, wR2 = 0.0739
Final R indexes [all data]	R1 = 0.0345, wR2 = 0.0783
Largest diff. peak/hole / e Å-3	0.27/-0.31

2(b).3.6 Representative Characterization Data for Complex C-6

Cr $(CO)_6$ (0.1320 g, 0.6mmol) was added to an oven dried Schlenk tube already charged with 3ml Toluene solution of Xanthphos (0.2893 g, 0.5 mmol) inside the glove box. Schleck was taken out of the glove box and placed in a pre-heated oil bath at 120 °C for 48 hours. Afterwards the reaction was stopped and allowed to cool at room temperature, yellowish solution was obtained which was filtered and dried under vacuum. Resulted residue was washed with hexane twice and dried overnight, yellow crystalline powder was obtained (70%) yield. Single crystals suitable for diffraction were obtained by diffusing hexane in saturated DCM solution of compound.

^{1}H NMR (500 MHz, $CDCl_3$) δ 7.45 (2H, d) 7.20-7.11 (20H), 7.02 (2H, t), 1.55 (6H, t).
^{13}C NMR (126 MHz, $CDCl_3$) δ 226.18 (m), 221.15 (t), 137.91, 134.78 (m), 132.93 (t), 130.54, 129.26, 128.17 (t), 126.92, 125.34, 123.95 (m), 123.44, 35.59, 28.83.
^{31}P NMR (203 MHz, $CDCl_3$) δ 39.84.
FT-IR cm^{-1} 2000 (CO), 1878 (CO), 1856 (CO).
HRMS $C_{43}H_{32}CrO_5P_2$ Calculated 742.1130. Found 742.0891

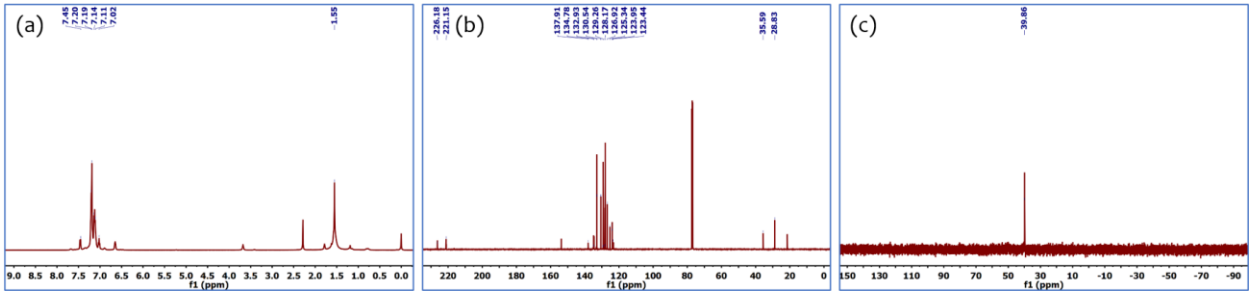
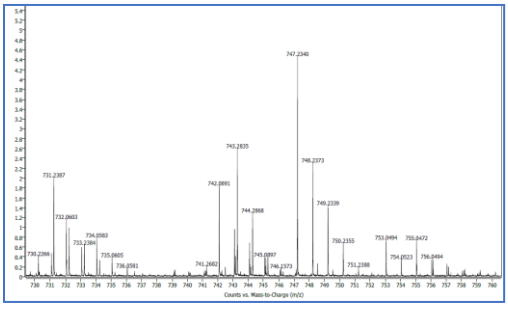
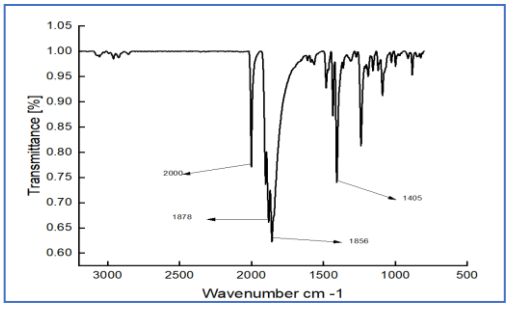


Fig. 2(b).3.6 (a) ^{1}H NMR Spectrum, **(b)** ^{13}C Spectrum, **(c)** ^{31}P Spectrum for **C-6** complex.

(d)





(e)

Fig. 2(b).3.6 (d) ESI-MS Spectrum, **(e)** FTIR Spectrum for **C-6** complex.

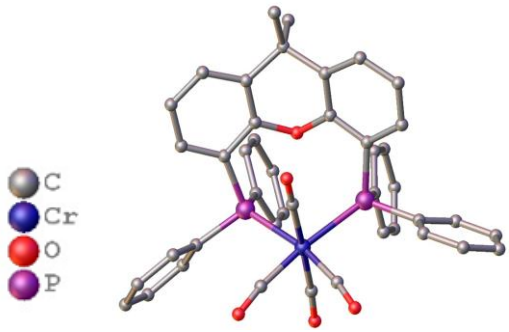


Fig. 2(b).3.6 (f) ORTEP Drawing of **C-6** complex.

Table 2(b).5 Crystal data and structure refinement for **C-6.**

CCDC no.	2309758

Empirical formula	C43H32CrO5P2
Formula weight	742.62
Temperature/K	296.0
Crystal system	triclinic
Space group	P-1
a/Å	11.116(5)
b/Å	11.652(6)
c/Å	15.549(8)
α/°	103.511(12)
β/°	101.950(12)
γ/°	100.896(12)
Volume/Å3	1855.1(15)
Z	2
ρcalcg/cm3	1.329
μ/mm-1	0.440
F(000)	768.0
Crystal size/mm3	0.15 × 0.12 × 0.1
Radiation	MoKα (λ = 0.71073)
2Θ range for data collection	3.868 to 50.09
Index ranges	-13 ≤ h ≤ 13, -13 ≤ k ≤ 13, -18 ≤ l ≤ 18
Reflections collected	35327
Independent reflections	6525 [Rint = 0.0291, Rsigma = 0.0194]
Data/restraints/parameters	6525/0/462
Goodness-of-fit on F2	1.120
Final R indexes [I>=2σ (I)]	R1 = 0.0411, wR2 = 0.0892
Final R indexes [all data]	R1 = 0.0497, wR2 = 0.0973
Largest diff. peak/hole / e Å-3	0.30/-0.37

2(b).3.7 Representative Characterization Data for Complex C-7

Cr $(CO)_6$ (0.030 g, 0.136mmol) was added to an oven dried Schlenk tube already charged with 4ml Toluene solution of DCYPP (0.050 g, 0.114 mmol) inside the glove box. Schleck was taken out of the glove box and placed in a pre-heated oil bath at 120 °C for 48 hours. Afterwards the reaction was stopped and allowed to cool at room temperature, greenish solution was obtained which was filtered and dried under vacuum. Resulted residue was washed dissolved in DCM and extracted twice with water. Methanol was added to the DCM layer and left for few days. Green coloured needles were obtained. (50%) yield.

^{1}H NMR (500 MHz, $CDCl_3$) δ 2.04 (4H, t), 1.89(4H, d), 1.76-1.60 (16H, m), 1.40 (8H, sext), 1.28 (8H, sext), 0.96-0.86(8H, m).
^{13}C NMR (126 MHz, $CDCl_3$) δ 227.59 (m), 223.59 (t), 39.99 (m), 28.71, 27.62 (m), 26.32, 21.61(m), 20.06 (t).
^{31}P NMR (203 MHz, $CDCl_3$) δ 40.39.
FT-IR cm^{-1} 1991 (CO), 1925 (CO), 1852 (CO).
HRMS $C_{31}H_{50}CrO_4P_2$ Calculated 600.2598. Found 600.2584.

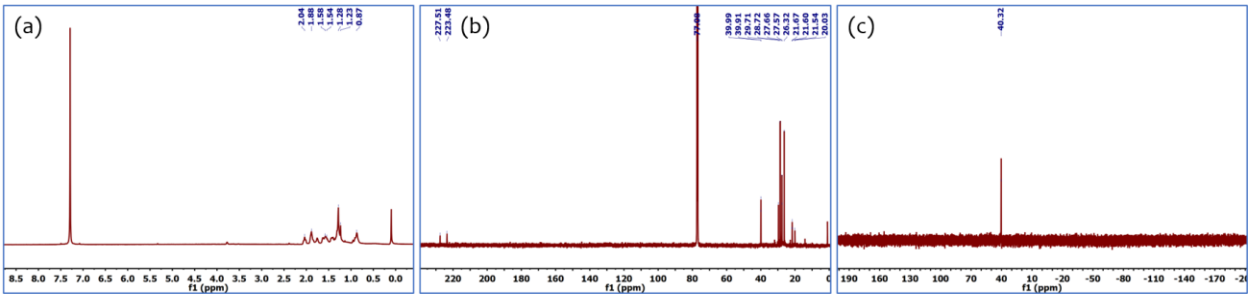
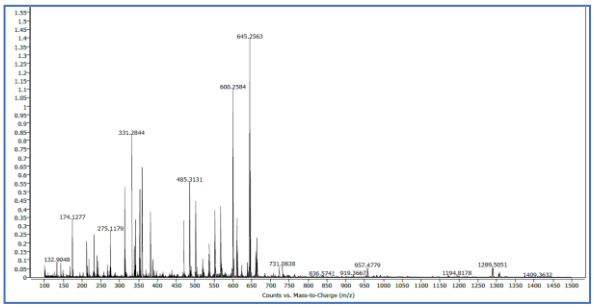
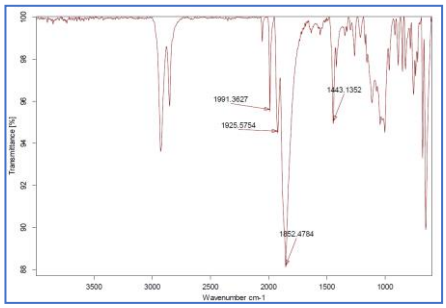


Fig. 2(b).3.7 (a) ^{1}H NMR Spectrum, **(b)** ^{13}C Spectrum, **(c)** ^{31}P Spectrum for **C-7** complex.

(d)





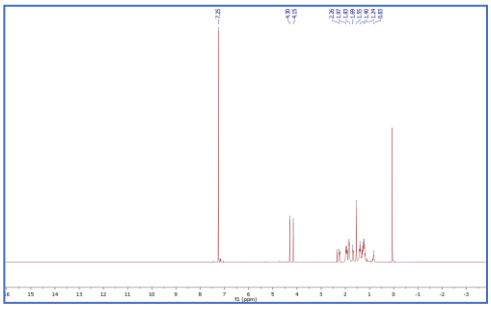
(e)

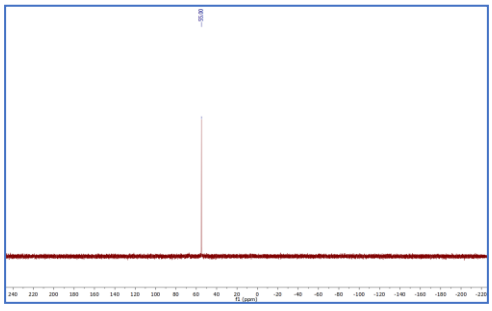
Fig. 2(b).3.7 (d) ESI-MS Spectrum, **(e)** FTIR Spectrum for **Cr-7** complex.

2(b).3.8 Representative Characterization Data for Complex C-8

$CrDiPPF(CO)_4$ (**C-8**)
^{1}H NMR (500 MHz, $CDCl_3$) δ 4.35 (4H), 4.30 (4H), 2.26 m (4H), 1.97-1.24 m (24H).
^{31}P{^{1}H}-NMR (203.0 MHz, $CDCl_3$) δ 55.00 (2P).

(a)





(b)

Fig. 2(b).3.8 (a) ^{1}H NMR Spectrum, **(b)** ^{31}P Spectrum for **C-8** complex.

2(b).3.9 Representative Characterization Data for Complex C-9

HRMS $C_{10}H_{16}CrN_2O_4$, Exact Mass: 280.0515 Found 280.0966.

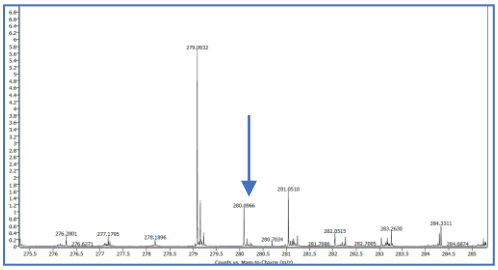


Fig. 3(b).3.9 ESI-MS Spectrum for **C-9** complex.

2(b).3.10 Representative Characterization Data for Complex C-10

HRMS $C_{16}H_8CrN_2O_4$, Exact Mass: 343.9889 Found 343.2953.

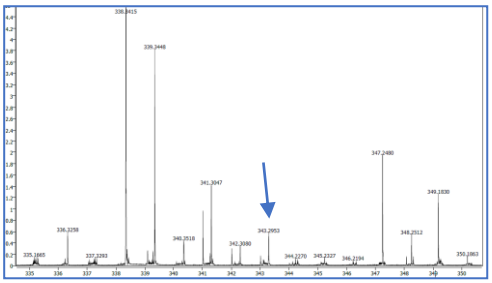
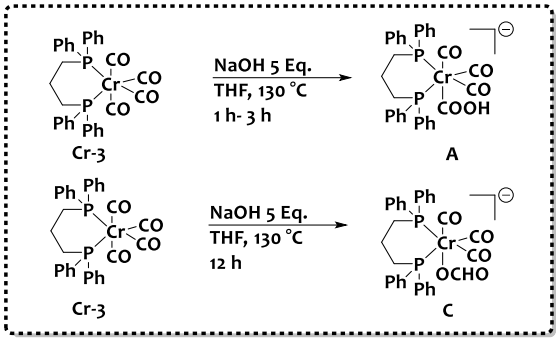


Fig. 2(b).3.10 ESI-MS Spectrum for **C-10** complex.

2(b).3.11 Mechanistic Experiments.



Scheme 2(b).3 Scheme for mechanistic experiments.

a

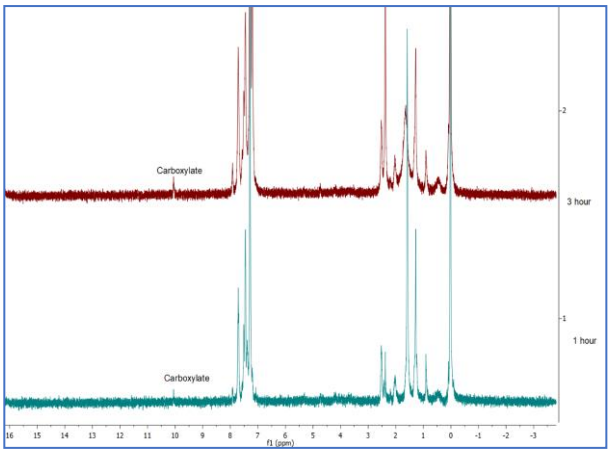


Fig. 2(b).3.11 (a) Stacked ^1H NMR for identifying intermediate A formed by the reaction of **C-3** with 5 Eq. NaOH after 1 hour and 3 h reaction time.

(b)

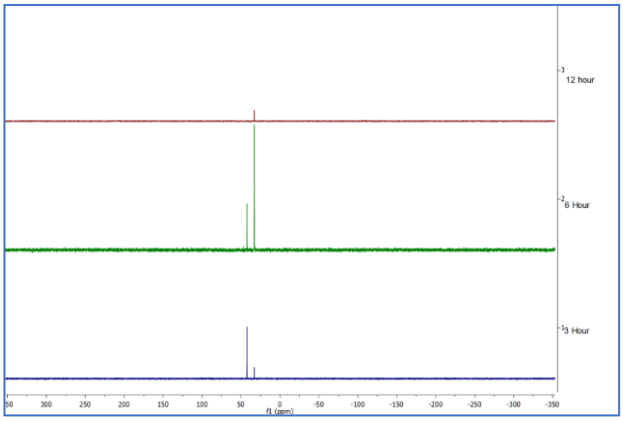


Fig. 2(b).3.11 (b) Stacked ^{31}P NMR for Stacked ^{31}P NMR recorded after 3h, 6h, and 12h respectively for the reaction of **C-3** with 5 Eq NaOH.

(c)

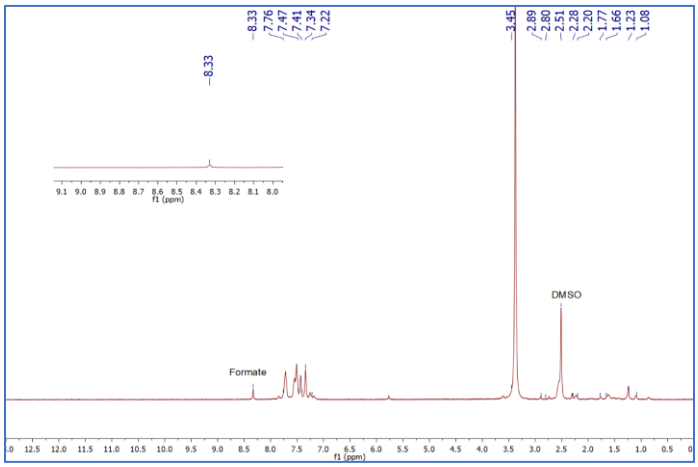


Fig. 2(b).3.11 (c) ^{1}H NMR for the reaction of **C-3** and NaOH base after 12 h reaction time.

(d)

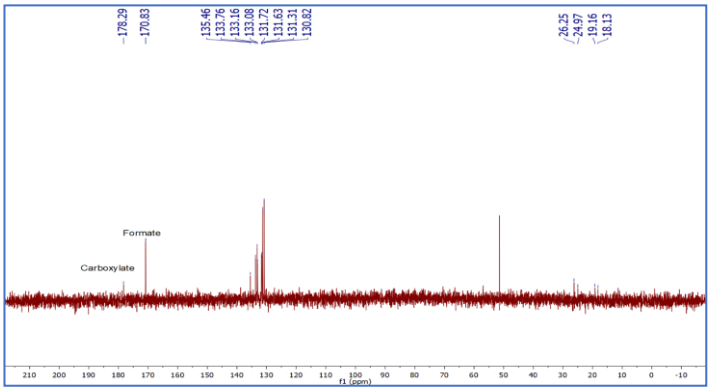
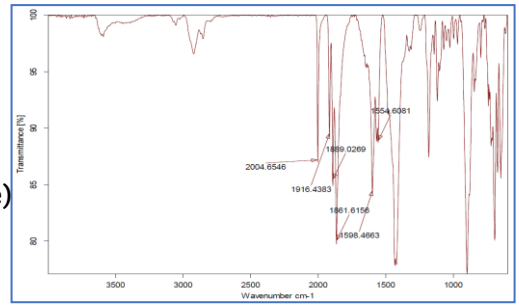
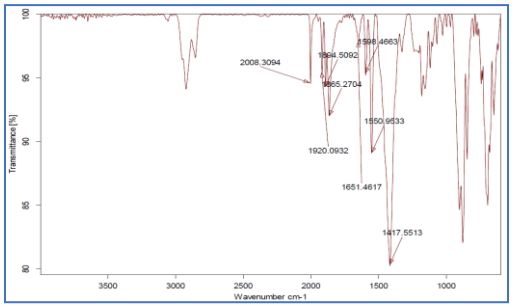


Fig. 2(b).3.11 (d) ^{13}C NMR for the reaction of **C-3** and NaOH base after 12 h reaction time.

(e)

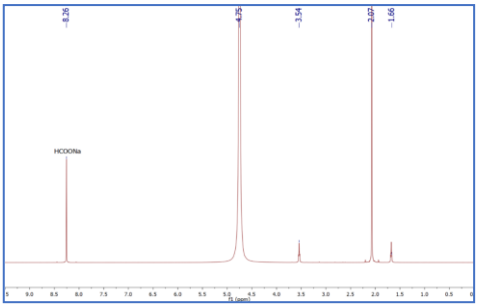


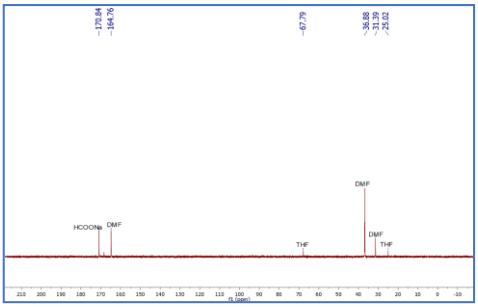


(f)

Fig. 2(b).3.11 (e) FTIR Spectrum for the reaction of **C-3** and NaOH base after 3 h reaction time, **(f)** FTIR Spectrum taken after 12 h reaction time.

(g)





(h)

Fig. 2(b).3.11 (g) Representative ^{1}H NMR, **(h)** ^{13}C NMR for Cr Catalyzed carbon dioxide hydrogenation to formate.

2(b).4 Computational Details

All the calculations were performed out using the ORCA package.[11] Geometry optimizations were carried out using local density Minnesota functional (M06L). Solvent (tetrahydrofuran) effects have been included in our calculations using the conductor-like polarizable continuum model (CPCM).[12-13] The SDD (MDF10) basis set with an effective core potential for Cr and the 6-311++G** basis set were used in all calculations. In addition, we used other combinations for geometry optimization, B3LYP/6-31G** (for other elements except Cr) and M06L/6-31G**[14] (for other elements except Cr) for all intermediates in both mechanisms. Vibrational normal modes and harmonic frequencies for stationary structures were obtained through the diagonalization of the ground state energy second derivative matrix. Harmonic vibrational frequencies were calculated to confirm the local minimum energy structures. Zero-point energy and thermal corrections have been included in our reaction free energy calculations under T = 298.15 K and 1 atm pressure conditions. The reaction free energies (ΔG) were calculated from the free energy difference between the final and initial states. Harmonic vibrational frequencies were calculated to characterize the nature of stationary points. Transition states (TSs) were characterized due to the presence of an imaginary vibrational frequency. The NEB-TS[15] method in ORCA was used to find the transition states.

Table 2(b).6 Optimized Stationary point energies for proposed Mechanism-1 (M1) using M06L and B3LYP density functionals utilizing 6-31G**[SDD/ECP(Cr)]16 basis set. All energies in kcal/mol.

Stationary Point	M06L	B3LYP
C-3 + $2Na^+$ + $2OH^-$ + H2 + THF + CO_2	0.0	0.0
A + $2Na^+$ + OH^- + H_2 + THF + CO_2	-31.9	-32.4
B + $2Na^+$ + OH^- + H_2 + THF + $2CO_2$	-43.1	-37.9
TSBC + $2Na^+$ + OH- + H_2 + THF + CO_2	-40.1	-36.3
C + $2Na^+$ + OH^- + H_2 + THF + CO_2	-57.5	-55.5
D + $HCOO^-$ + $2Na^+$ + OH^- + H_2 + CO_2	-38.5	-33.3
E + HCOO- + $2Na^+$ + OH^- + THF +CO_2	-36.0	-35.1
B + $HCOO^-$ + $2Na^+$ + H_2O + THF +CO_2	-88.7	-85.3

Table 2(b).7 Optimized Stationary point energies for proposed Mechanism-2 (M2) using M06L and B3LYP density functionals utilizing 6-31G**[SDD/ECP(Cr)] basis set. All energies in kcal/mol.

Stationary Point	M06L	B3LYP
C-3 + $2Na^+$ + $2OH^-$ + H_2 + THF + CO_2	0.0	0.0
V + $2Na^+$ + $2OH^-$ + H_2 + THF + CO_2 + CO	33.3	22.8
D+$2Na^+$ + $2OH^-$ + H_2 + CO_2 + CO	24.4	24.0
E + $2Na^+$ + $2OH^-$ + THF + CO_2 + CO	26.9	24.7
B + $2Na^+$ + OH^- + H2O +	-25.8	-25.4

THF + CO_2 + CO		
TSBC + $2Na^+$ + OH^- + H_2O + THF + CO	-22.8	-23.8
C + $2Na^+$ + OH^- + H_2O + THF + CO	-40.1	-43.0
V + $HCOO^-$ + $2Na^+$ + OH^- + H_2O + THF + CO	-12.2	-24.6

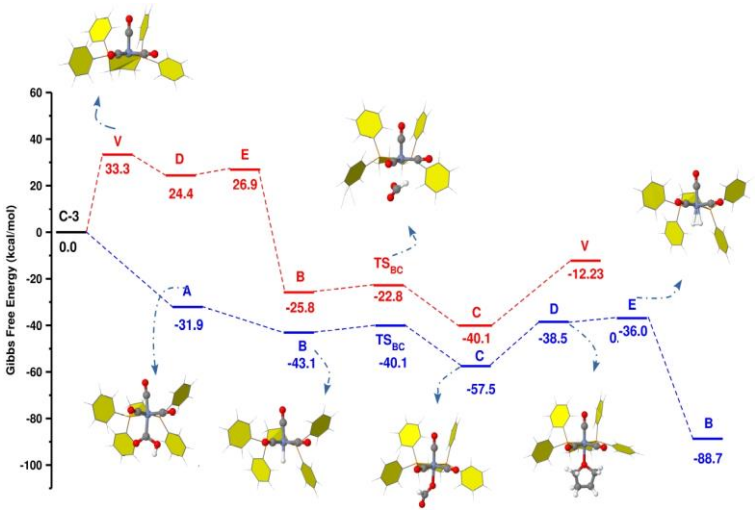


Fig.2(b).4 (a) M06L/631G**[SDD/ECP(Cr)] optimized stationary points comparison between possible mechanisms M1(blue) and M2(Red). For stationary point information see Table 3(b).6 and 3(b).7.

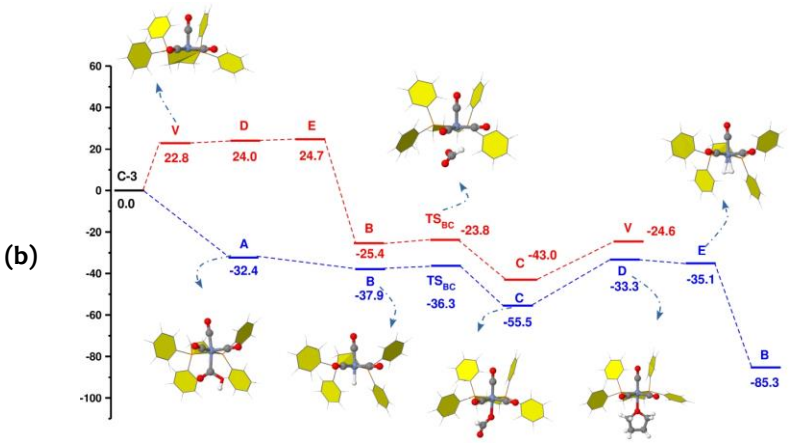
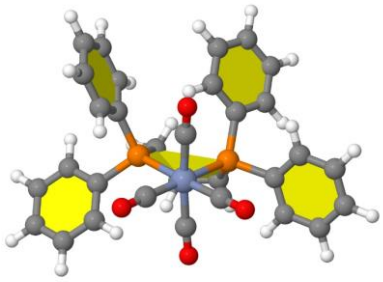
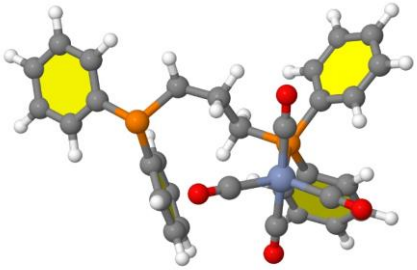
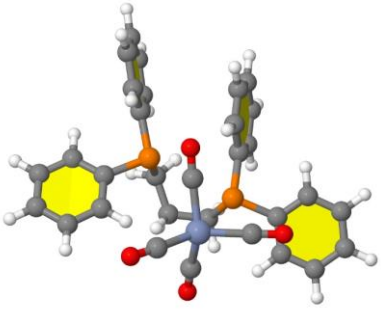


Fig.2(b).4 (b) B3LYP/631G**[SDD/ECP(Cr)] optimized stationary points comparison between possible mechanisms M1(blue) and M2(Red). For stationary point information Table 3(b).6 and 3(b).7.

Table 2(b).8 The optimized geometries and relative energies of C-3 complex in singlet, triplet and quintet spin states.

C-3 spin state	Geometry	Energy (kcal/mol)

Singlet		0.0
Triplet		42.0
Quintet		75.4

2(c)

Pincer Chromium (II) Catalysed Hydrogenation of CO_2, Bicarbonate to Formates

Research Article based on this study:

Singh, T.; Chakraborty, S. Pincer Chromium (II) Catalysed Hydrogenation of CO_2, Bicarbonate to Formate (Manuscript Submitted).

2(c).1 Introduction

In recent years pincer complexes have evolved as an elegant class of homogeneous catalysts in executing numerous environmentally benign sustainable chemical transformations.[242-243] Pincer ligands bearing multiple donor sites often possess the meridional geometry around the metal centre and influence the steric and electronics of the metal complexes. The ligand systems are also tunable, have well-built chelating potential, and exhibit hemilabile properties.[244] The direct involvement of the pincer ligands in bond making and bond breaking processes via synergistic metal-ligand cooperation (MLC) without affecting the formal oxidation state of the metal centres are also notable features of these systems.[54,245-246,247-248] Seminal discoveries on MLC by Shvo, Noyori, and Milstein involving O-H/N-H/C-H bonds of the ligand ushered unconventional reactivities and catalytic efficiency.[178-179,249-251] Particularly, the amido-amine MLC of amine ligands discovered by Noyori[249,251] resulted in the development of next generation pincer PNP ligand-based metal complexes for effective catalytic transformations.[180,252] This has led to remarkable explosion in homogeneous (de)hydrogenation reactions of catalytically challenging functionalities relevant for commercial applications.[253]

Catalytic hydrogenation is an atom-economic, greener, and sustainable methodology.[177] However, major class of homogeneous catalysts are based on platinum group metals, which are potentially toxic, expensive rare-earth metals and facilitate two electron redox processes.[2,10] Probing earth-abundant, cost-effective, less toxic 3d transition metal complexes in homogeneous catalysis is of current interest to the scientific community.[50,52] Nevertheless, these metals possess multiple spin states, and distinct coordination geometries, react by following one electron redox mechanism and bestow substitutional lability.[57] The advent of metal-ligand cooperation concept resulted in noteworthy advancements on the implementation of 3d pincer complexes catalyzed hydrogenation reactions.[53-56] In this regard utilization of chromium is also attractive on account of its biocompatibility and ready-availability.[182,255] In fact commercially, chromium-based Phillips catalyst is extensively employed to meet the 40% of the global demand for high-density polyethylene.[261-262] Chromium complexes are known to mostly catalyze isomerization, oligomerization, coupling reactions and oxidation reactions.[181-182,256-260] Very recently dehydrogenative coupling reactions have also been explored.[222-226] Hydrogenation of ketones, aldehydes, polycyclic aromatic hydrocarbons as well as the semi-hydrogenation of alkynes were reported [229,263-269]

In light of the closed cycle economy[24] and need for renewable hydrogen storage materials, hydrogenation of CO_2 to formic acid/formate is highly sought after.[29,71] Formic acid (FA) is considered to be an attractive molecule with broad applications in chemical industries. However, the commercial manufacture of FA relies on non-renewable fossil feedstock, and thus alternative protocols to obtain FA from renewable resources like CO_2 or biomass are highly desirable and has drawn considerable scientific attention.[63-67,143] A vast array of homogeneous catalysts have emerged for the hydrogenation of CO_2 to formic acid or formate showcasing extraordinary efficiencies.[32,44,58,221] A variety of 3d metal catalyzed hydrogenation of carbon

dioxide to formic acid/formate were also reported.[58,86-88,92,94-96,102,105-107,111-113,116,117,119,121,124,126,139,202,226] Notably, PNP ligand-based first row complexes featured excellent TONs as shown in Figure 2(c)1. Seminal report on Cr catalyzed hydrogenation of CO_2 to alkyl formate was demonstrated by Darensbourg in 1984 utilizing an anionic chromium hydridocarbonyl complex in alcoholic solvent giving a very low TON of 14.6.[128] Recently, we have disclosed a series of bidentate phosphine ligands derived chromium complexes for CO_2 hydrogenation, and achieved a maximum TON of 2,59000 for the formate formation.[134] Instigated by this state of the art discovery and our recent findings on CO_2 hydrogenation, we were curious to dig into catalytic performance of literature known pincer-PNP tethered chromium complexes Fig 2(c).1 Herein, we report an effective chromium PNP pincer catalyst **C-1** for the hydrogenation of CO_2 and biologically relevant $NaHCO_3$ to formate.

.

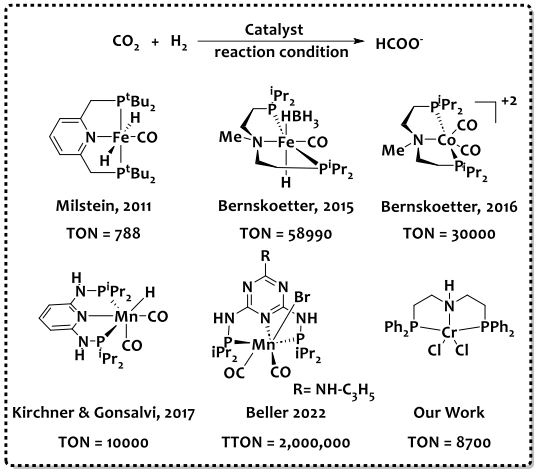


Fig. 2(c).1 3d metal PNP pincer complexes known for CO_2 hydrogenation.

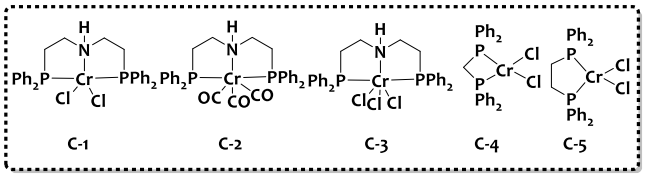


Fig. 2(c).2 Chromium complexes explored for CO_2 hydrogenation.

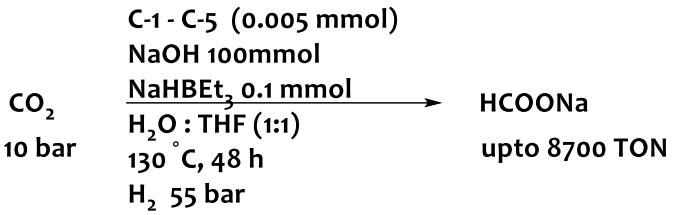
2(c).2 Results and Discussion

(**C-1 to C-5**) were prepared according to literature procedures [270-273]. **C-1** is known to be active for ethylene polymerisation reactions.[270] However, the catalytic potential of the catalyst in hydrogenation reaction was not explored. At the outset, 0.005 mmol **C-1** was used in the hydrogenation of CO_2 in the presence of 0.10 mmol $NaHBEt_3$ (1 M in toluene), NaOH at 130 ^{0}C in 1:1 THF/H_2O mixture at the expense of a total 65 bar (1:5.5 ratio of CO_2:H_2) pressure resulting in a TON of 8700 (Table 2(c).1, entry 1). When the tricarbonyl complex **C-2** (0.005 mmol) was probed for the hydrogenation reaction, TON dropped significantly to 204 (Table 2(c).1, entry 2). The trichloride complex **C-3** was found to be inferior and a formate TON of 330 was recorded (Table 2(c).1, entry 3). $Cr(DPPM)Cl_2$ (**C-4**, DPPM((1,1-Bis(diphenylphosphino)methane) displayed improved activity comparatively and yielded formate with 1708 (Table 2(c).1, entry 4). Shifting the catalytic species towards **C-5** $Cr(DPPE)Cl_2$ (DPPE=1,2-Bis(diphenylphosphino)ethane) resulted in formate formation with a TON of 1566 (Table 2(c).1, entry 5). Trace amount of formate was achieved upon carrying the reaction without catalyst and $NaHBEt_3$, (Table 2(c).1, entry 6). $CrCl_2$ was also screened as catalyst and formate TON of 1304 was recorded (Table 2(c).1, entry 7) indicating the crucial role of the PNP MACHO ligand.

.

Having the most efficient catalyst **C-1** in our hand**,** we embark on the optimization studies further by lowering the amount of $NaHBEt_3$. Accordingly, decreasing the loading of $NaBHEt_3$ to 0.05 mmol and a TON of 1700 was documented (Table 2(c).1, entry 8). TON decreased further to 1620 while using 0.025 mmol $NaHBEt_3$ in the reaction (Table 2(c).1, entry 9). When the reaction was conducted without any additives, TON of 1182 (Table 2(c).1, entry 10) was attained. Furthermore, NaHMDS and *t*-BuOK (Table 2(c).1, entry 11-12) were also tested in place of $NaHBEt_3$ and TONs of 524 and 2428 were recorded, respectively. Taking 0.1 mmol $NaHBEt_3$ as catalyst resulted in formation of formate with negligible TON (Table 2(c).1, entry 13).

Table2(c).1 Chromium catalyzed CO_2 hydrogenation to formate.[a]



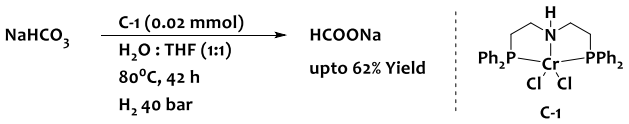
Entry	Base	Catalyst	Pressure	Solvent	TON[b,c]
1	NaOH	**C-1**	10:55	THF:H_2O	8700
2	NaOH	**C-2**	10:55	THF:H_2O	204
3	NaOH	**C-3**	10:55	THF:H_2O	330
4	NaOH	**C-4**	10:55	THF:H_2O	1708
5	NaOH	**C-5**	10:55	THF:H_2O	1566
6	NaOH	**-**	10:55	THF:H_2O	Trace
7[c]	NaOH	**$CrCl_2$**	10:55	THF:H_2O	1304
8[d]	NaOH	**C-1**	10:55	THF:H_2O	1700
9[e]	NaOH	**C-1**	10:55	THF:H_2O	1620
10[f]	NaOH	**C-1**	10:55	THF:H_2O	1182
11[g]	NaOH	**C-1**	10:55	THF:H_2O	524
12[h]	NaOH	**C-1**	10:55	THF:H_2O	2428
13[i]	NaOH	**-**	10:55	THF:H_2O	5
14[j]	Et_3N	**C-1**	10:55	THF:H_2O	Trace
15[k]	DBU	**C-1**	10:55	THF:H_2O	Trace
16[l]	Na_2CO_3	**C-1**	10:55	THF:H_2O	Trace
17[m]	Et_3N	**C-1**	10:55	THF:H_2O	Trace

18[n]	DBU	**C-1**	10:55	THF:H_2O	Trace
19	NaOH	**C-1**	10:55	Toluene	836
20[0]	NaOH	**C-1**	10:55	THF	42
21	NaOH	**C-1**	10:55	H_2O	7674
22[P]	NaOH	**C-1**	10:55	THF:H_2O	3050
23	NaOH	**C-1**	10:30	THF:H_2O	1018

[a]Reaction conditions: Unless and otherwise stated 130 °C, 55 bar H_2 at room temperature, 10 bar CO_2, 48 h, 100 mmol NaOH, certain mmol catalyst. $NaHBEt_3$ 0.1 mmol. [b]Yield based on ^1H NMR signals of sodium formate, with DMF used as an internal standard. [c]Turnover number = moles of sodium formate per mole of catalyst. [d]0.05 mmol $NaHBEt_3$ was taken. [e]0.025mmol $NaHBEt_3$ was taken.[f] No additive was taken.[g]0.1mmol NaHMDS was taken as additive. [h]0.1mmol *t*-BuOK was taken.[i]reaction was performed in absence of C-1 using 0.1mmol $NaHBEt_3$.[j] 35mmol Et_3N was taken.[k]35mmol DBU was taken.[l]50mmol Na_2CO_3 was taken.[m] 0.1mmol NaOH was also added. [n] 0.1mmol NaOH was also added.[O] 20 mmol NaOH was taken. [P]Reaction was done for 24 h.

Base screening was also carried out to improve the yield of the reaction. To our surprise, when the base was changed from NaOH to Et_3N (35 mmol), trace amount of product was obtained (Table 2(c).1, entry 14). Further, DBU (35 mmol) and Na_2CO_3 (50 mmol) also furnished trace amount of the corresponding formate salts as revealed by the NMR (Table 2(c).1, entries 15-16). Reactions were also conducted using DBU and Et_3N as bases in the presence of 0.1 mmol NaOH as additive. However, in these cases the corresponding formate products were obtained in trace amount only (Table 2(c).1, entry 17-18). Solvent optimization was also performed. When the reaction was carried out in toluene and THF (in the presence of 20 mmol NaOH) and water separately, TONs of 836, 42 and 7674 were obtained, respectively (Table 2(c).1, entries 19-21). When the reaction was carried out for 24 h, the formate TON dropped to 3050 (Table 2(c).1, entry 22). Likewise, performing the reaction with 10:30 (CO_2:H_2) pressure under optimum conditions provided formate with 1018 TON (Table 2(c).1, entry 23).

Table2(c).2 Chromium catalyzed hydrogenation of sodium bicarbonate.[a]

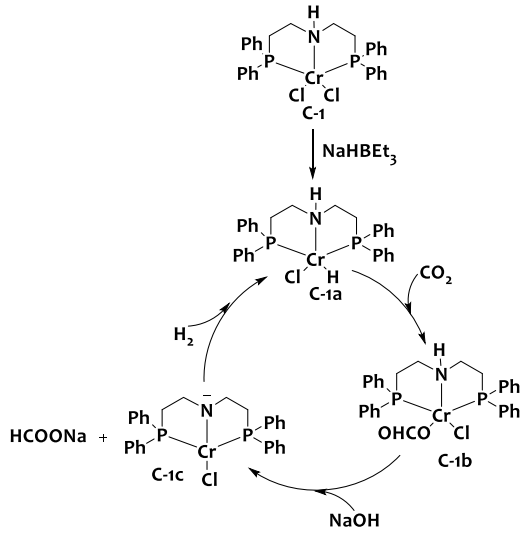


Entry	Base	Catalyst	Temperature	Solvent	Yield[b]
1	-	**C-1**	80°C	THF:H_2O	33%
2[c]	-	**C-1**	80°C	THF:H_2O	18%
3	-	**C-1**	120°C	THF:H_2O	24%
4	-	**-**	80°C	THF:H_2O	Trace
5	*t*-BuOK	**C-1**	80°C	THF:H_2O	39%
6	NaOH	**C-1**	80°C	THF:H_2O	29%
7	NaHMDS	**C-1**	80°C	THF:H_2O	62%

[a]Reaction conditions: NaHCO3 0.5 mmol, 80 °C, 40 bar H_2, 42 h, 0.02mmol catalyst (C-1),[b]Yield based on ^{1}H NMR signals of sodium formate with DMF used as an internal standard.[c] 60 bar hydrogen is taken.

In contrast to the reduction of CO_2, less research attention has been paid on the biologically important reduction of bicarbonates, and the reported activity of hydrogenation catalysts are substantially lower.[88] We were intrigued to assess the catalytic activity of **C-1** in sodium bicarbonate hydrogenation. A loading of 2 mol% catalyst **C-1** upon charging 40 bar H_2 after 42 h at 80 °C in THF:H_2O mixture hydrogenated sodium bicarbonate to sodium formate with 33% yield (Table 2(c).2, entry 1). Formate yield decreased to 18% when 60 bar H_2 pressure was used (Table 2(c).2, entry 2). When the reaction was carried out at 120 °C, formate was obtained in 24% yield (Table 2(c).2, entry 3). Trace amount of formate product was achieved when the reaction was performed in the absence of catalyst (Table 2(c).2, entry 4). In order to generate active catalyst 10 mol% *t*-BuOK when scrutinized as an additive resulting in the formation of formate with 39% yield (Table 2(c).2, entry 5). Upon replacing *t*-BuOK with NaOH formate was procured with 29% yield (Table 2(c).2, entry 6). To our delight when NaHMDS was used as additive, formate yield improved to 62% (Table 2(c).2, entry 7).

To get the mechanistic insight on Cr catalyzed CO_2 hydrogenation, chromium complex **C-1** was examined for several stoichiometric reactions. Initially a THF solution of **C-1** was charged with 1 bar CO_2 and stirred at room temperature and then heated further to 80°C overnight. However, no change was observed as revealed by IR and HRMS studies. Reacting 2 equiv. $NaHBEt_3$ and heating to 80°C in the presence of **C-1** and 1 bar CO_2 produced green coloured solution after 5 h. Analyzing the reaction mixture by IR spectroscopy revealed a strong peak at 1653 cm^{-1}, which is comparable with related Mn, Mo formate complex reported in literature.[125] The reaction mixture was also analyzed with the aid of mass spectrometry and a molecular ion peak corresponding to a possible formate complex C-**1a** was identified. However, when the reaction of **C-1** was heated with 2 equiv. of $NaHBEt_3$ in the absence of CO_2 the solution turned turbid with the formation of precipitates. Upon analyzing the reaction mixture using IR, a weak signal at 1563 cm^{-1} was identified. The signal is in close proximity to a simulated IR data of a monohydride compound **C-1a** (Scheme 2(c).1). A molecular ion peak corresponding to **C-1a** was also detected in the HRMS study. It is worth mentioning that performing the reaction in presence of 5 equiv. $NaHBEt_3$ in THF at 80°C after 5 h resulted in the complex decomposition as confirmed by the appearance of a signal at -19.5 ppm in the ^{31}P NMR corresponding to free ligand.



Scheme 2(c).1 Proposed mechanism for **C-3** catalyzed CO_2 hydrogenation.

Based upon our experimental finding we proposed a mechanism outlined in scheme 2(c).1. Initially formation of monohydride complex **C-1a** took place which is supposed to be the active species for catalytic cycle. The M-H bond of **C-1a** in inserts CO_2 forming the formate complex **C-1b**. the formate complex **C-1b** in the presence of NaOH eliminates sodium formate with the generation of highly unstable monochloride complex **C-1c**, which finally in the presence of H_2 regenerates monohydride species **C-1a** and closes the catalytic cycle.

2(c).3 Experimental Section

The complexes **C-1, C-4, C-5,** were prepared by mixing the anhydrous $CrCl_2$ with respective bidentate phosphine & pincer ligands stoichiometrically in round bottom flask inside the glove box. The reaction was stirred at room temperature for 24 hours in THF. Afterwards reaction was stopped, solvent was dried under vacuum and the fine crystalline powder thus obtained was characterized, obtained data was in sync with the reported one. [270-273]

C-3 was prepared by mixing Anhydrous $CrCl_3$ with the PNP pincer ligand stoichiometrically in round bottom flask inside the glove box. The reaction was stirred at room temperature for 24 hours in THF. Afterwards reaction was stopped, solvent was dried under vacuum and the fine crystalline powder thus obtained was characterized, obtained data was in sync with the reported one.[273]

C-2 was prepared by Charging Schlenk flask with $Cr(CO)_6$ and Toluene solution of PNP pincer ligand stoichiometrically inside the glove box. Schlenk was taken out and reaction was heated to 120 °C for 48 hours. Afterwards reaction was stopped, cooled and dried under vacuum. Fine crystalline powder thus obtained was characterized, which matched with available data.[272]

2(c).3.1 Representative Characterization Data for Complex C-1

HRMS $C_{28}H_{29}Cl_2CrNP_2$ Calculated 563.0557 Found 563.3127.

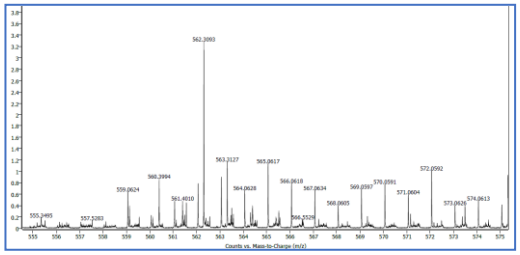
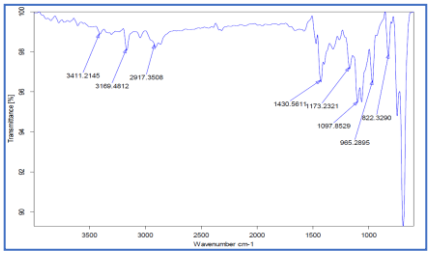
(a)   (b)

Fig. 2(c).3.1 (a) ESI-MS Spectrum, **(b)** FTIR Spectrum for **C-1** complex.

2(c).3.2 Representative Characterization Data for Complex C-2

HRMS $C_{31}H_{29}CrNO_3P_2$ Calculated 577.1028 Found 576.0681.

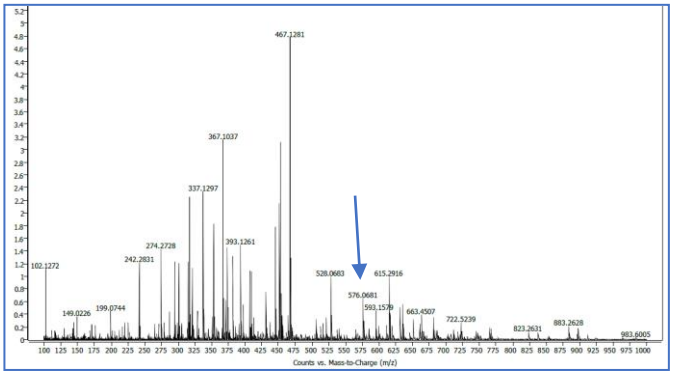


Fig. 2(c).3.2 ESI-MS Spectrum for **C-2** complex.

2(c).3.3 Representative Characterization Data for Complex C-3

HRMS $C_{28}H_{29}Cl_3CrNP_2$ Calculated 598.0246 Found 598.0544.

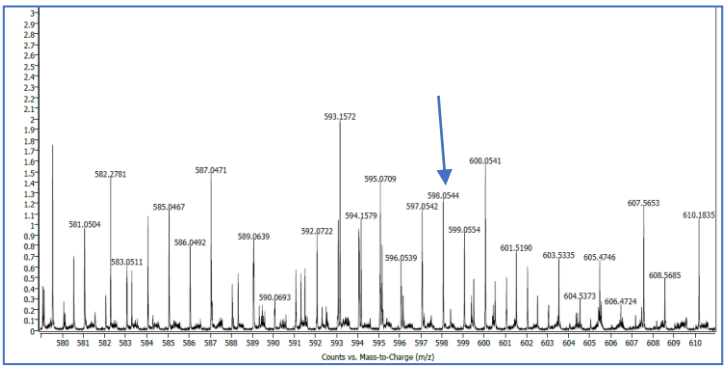


Fig. 3(c).3.3 ESI-MS Spectrum for **C-3** complex.

2(c).3.4 Representative Characterization Data for Complex C-4

HRMS $C_{25}H_{22}Cl_2CrP_2$ Calculated 505.9979 Found 505.4970.

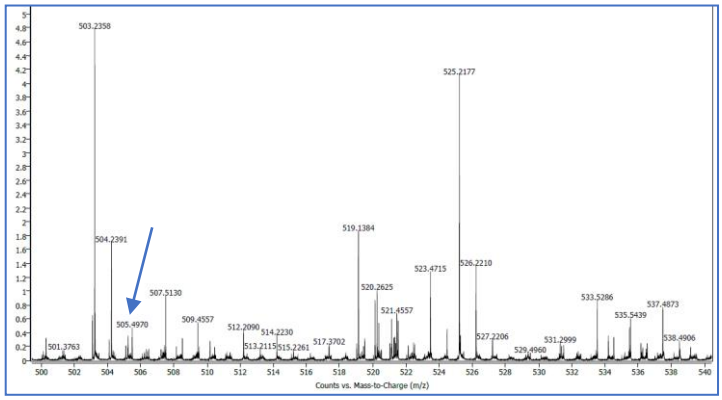


Fig. 2(c).3.4 ESI-MS Spectrum for **C-4** complex.

2(c).3.5 Representative Characterization Data for Complex C-5

HRMS $C_{26}H_{24}Cl_2CrP_2$ Calculated 520.0135 Found 520.2625.

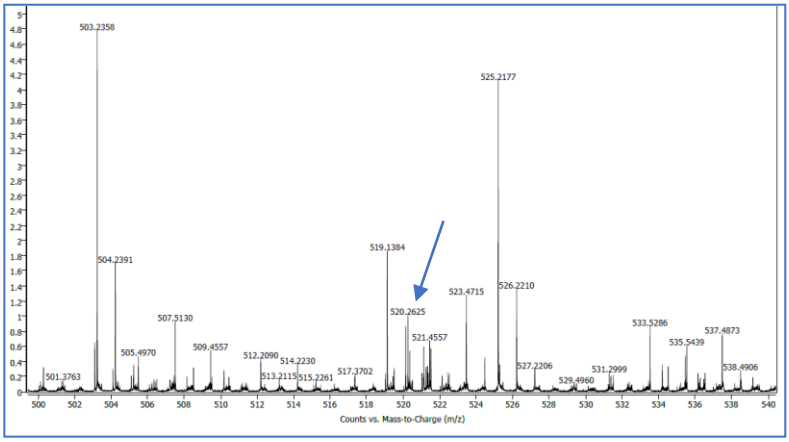
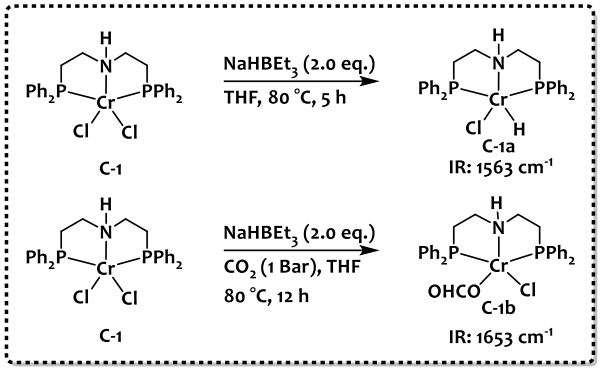


Fig. 2(c).3.5 ESI-MS Spectrum for **C-5** complex.

2(c).3.6 Mechanistic Experiments



Scheme 2(c).2 Scheme for mechanistic experiments.

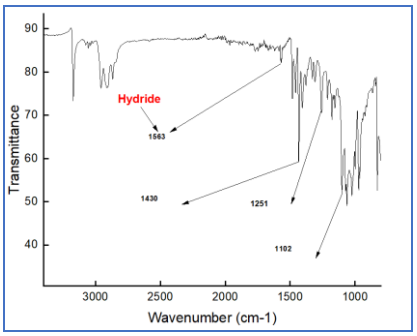


Fig. 2(c).3.6 FTIR Spectrum for the reaction of **C-1** and 2 eq. $NaHBEt_3$ heating at 80 °C after 5h.

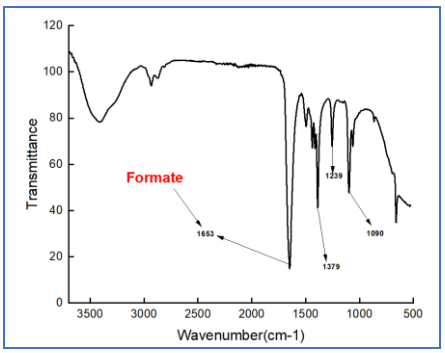


Fig. 2(c).3.7 FTIR Spectrum for the reaction of **C-1** and 2 eq. $NaHBEt_3$ in presence of 1 bar CO_2 heating at 80 °C after 12h.

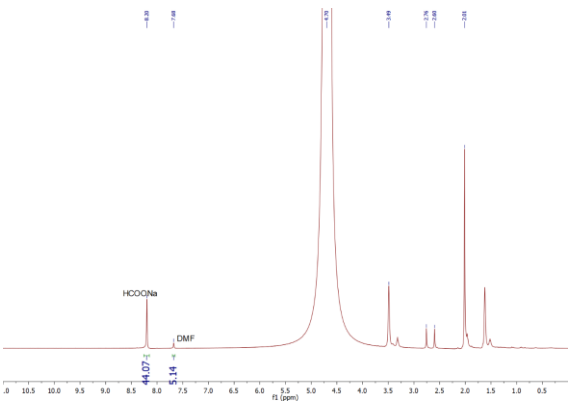


Fig. 2(c).3.8 Representative ^1H NMR for the **C-1** catalyzed CO_2 hydrogenation to formate.